Theses and Dissertations

2014

Computational Study of Multiple Hydrokinetic Turbine Performance

Joseph David Jonas
Lehigh University

Recommended Citation
Jonas, Joseph David, "Computational Study of Multiple Hydrokinetic Turbine Performance" (2014). *Theses and Dissertations.* Paper 1519.

Computational Study of

Multiple Hydrokinetic Turbine Performance

By

Joseph David Jonas

A Thesis

Presented to the Graduate and Research Committee

Of Lehigh University

in Candidacy for the Degree of Master of Science

in

Mechanical Engineering

Lehigh University

August 2014

This thesis is accepted and approved in partial fulfillment of the requirements for the Master of Science degree in Mechanical Engineering

_____

Date Approved

_____

Dr. Alparslan Oztekin
Thesis Advisor

_____

Dr. D. Gary Harlow, Chairperson
Mechanical Engineering and Mechanics

Table of Contents

List of Figures

Acknowledgements

The author would first like to thank his thesis advisor, Professor Alparslan Oztekin for his guidance, insight and enthusiasm through every step of this research process. Chris Schleicher and Jake Riglin, with their extensive knowledge of Computational Fluid Dynamics tools, were invaluable in assisting with simulation setup and troubleshooting, and the author would extend his gratitude to them as well. Additionally, the author would like to express his sincerest appreciation and thanks towards his parents and Lehigh University alumni Cynthia Ellsworth Jonas, BSME '82 and Gordon M Jonas, BSME '81 for all of their encouragement and wisdom over the last twenty-three years. Finally, the author would like to thank the myriad of other family, friends, teachers and mentors who have helped and continue to help him achieve his dreams.

Nomenclature

$\dot{KE}$	Rate of Kinetic Energy entering Turbine $[\text{J s}^{-1}]$
$\dot{m}$	Mass Flow rate entering Turbine $[\text{kg s}^{-1}]$
V_i	Velocity at Turbine Inlet $[\text{m s}^{-1}]$
ρ	Fluid Density $[\text{kg m}^{-3}]$
A	Swept Area of Turbine $[\text{m}^2]$
C_T	Ideal Turbine Power Coefficient [-]
V_o	Velocity at Turbine Exit $[\text{m s}^{-1}]$
P_{ideal}	Power Generated by Ideal Turbine [W]
TSR	Tip Speed Ratio [-]
R	Turbine Radius [m]
Ω	Magnitude of Rotation Rate of Turbine $[\text{rad s}^{-1}]$
σ	Solidity Ratio [-]
B	Number of Turbine Blades [-]
c	Chord length of turbine at blade tip [m]
Re_x	Reynolds Number based on characteristic length x [-]
x	Characteristic length of system [m]
μ	Dynamic Viscosity of Fluid [Pa s]
∇	Vector Differential Operator $[\text{m}^{-1}]$
$\cdot$	Vector Dot Product Operator [-]
$\boldsymbol{v}$	Absolute Velocity Vector $[\text{m s}^{-1}]$
t	Time [s]
p	Static Pressure [Pa]
$\boldsymbol{f}$	Net body force per Unit Volume Vector $[\text{N m}^{-3}]$
d	Turbine Separation Distance [m]
$\boldsymbol{v}_r$	Velocity Vector relative to rotating frame $[\text{m s}^{-1}]$
$\boldsymbol{\Omega}$	Vector of Revolution of the Rotating Domain $[\text{s}^{-1}]$
$\times$	Vector Cross Product [-]
$\boldsymbol{r}$	Displacement Vector from point in Rotating domain to origin of rotating domain (m)
k	Specific Turbulent Kinetic Energy $[\text{m}^2 \text{ s}^2]$
u_i	The i-th component of vector $\boldsymbol{v}$ $[\text{m s}^{-1}]$
$u_i{}'$	The fluctuating component of u_i $[\text{m s}^{-1}]$
ϵ	Specific Turbulent Dissipation $[\text{m}^2 \text{ s}^3]$
ν	Kinematic Viscosity (equal to μ/ρ) $[\text{m}^2 \text{ s}^{-1}]$
x_k	k-th component of the coordinate frame [m]
ω	Specific Dissipation Rate $[\text{s}^{-1}]$
β^*	Constant [0.09]
τ_{ij}	Reynolds Stress Tensor [Pa]
δ_{ij}	Kronecker delta function [-]
μ_t	Turbulent Dynamic Viscosity [Pa s]
F_1	Blending Function [-]
F_2	Blending Function [-]
$CD_{k\omega}$	Positive portion off-diagonal Cross Diffusion terms from ω equation $[\text{kg m}^{-3} \text{ s}^{-2}]$
Ω^*	Absolute value of Vorticity

	Vector [s^{-1}]		and outlet [s^{-1}]
σ_{k1}	Constant [0.85]	I	Turbulent Intensity [-]
σ_{k2}	Constant [1.0]	l	Turbulent Length Scale [-]
$\sigma_{\omega 1}$	Constant [0.5]	D_h	Hydraulic Diameter of River Domain [m]
$\sigma_{\omega 2}$	Constant [0.856]		
β_1	Constant [0.0750]	Re_{D_h}	Reynolds Number using D_h as the characteristic length [-]
β_2	Constant [0.0828]		
κ	Constant [0.41]	k_{wall}	Value of k at the solid walls of domain [$m^2\ s^2$]
a_1	Constant [0.31]		
γ_1	Function of β_1, β^*, $\sigma_{\omega 1}$, and κ [0.533166]	ω_{wall}	Value of ω at the solid walls of domain [s^{-1}]
γ_2	Function of β_2, β^*, $\sigma_{\omega 2}$, and κ [0.44035]	Δy_1	Distance from the wall to the nearest point in the discretized domain[m]
σ_k	Function of F_1, σ_{k1}, and σ_{k2} [-]	y^+	Dimensionless wall distance [-]
σ_ω	Function of F_1, $\sigma_{\omega 2}$ and $\sigma_{\omega 2}$ [-]	u_*	Friction Velocity [m s^{-1}]
β	Function of F_1, β_1, and β_2 [-]	τ_w	Wall shear stress [Pa]
γ	Function of F_1, γ_1, and γ_2 [-]	C_P	Coefficient of Performance [-]
U	Free Stream Velocity [m s^{-1}]	P	Simulation Power Output [W]
k_{io}	Value of k at the domain inlet and outlet [$m^2\ s^2$]	C_D	Coefficient of Drag [-]
		F_D	Simulation Drag [N]
ω_{io}	Value of ω at the domain inlet		

Abstract

The k-ω Shear Stress Transport turbulence model was used to determine the performance of a pair of horizontal-axis hydrokinetic turbines. By varying the separation distance perpendicular to the flow direction between these turbines and computing both power and drag coefficients, the relationship between these outputs and the separation distance as an input was discovered. This study used a rotating reference frame, steady state approximation over three separation distances and two different mesh sizes to verify mesh independence. Once this meshing methodology was verified, two more separation distances were run using the same steady-state approximations at the coarse mesh size to better understand turbine performance at greater separation distances. The results of these simulations show that, at a given separation distance, the left and right turbines have very similar performance. The power and drag coefficients were both found to decrease on the order of 8% as the turbines are brought closer together, which means that, in an infinite and uniform flow field, turbines should be placed as far apart as is feasible to maximize resultant combined power output.

1.   Introduction

1.1   History of Hydro Power

The potential for the movement of water to do useful work was realized thousands of years ago by farmers in Mesopotamia and ancient Egypt, whose advances in controlled irrigation allowed their civilizations to thrive in even harsh environments. Centuries later, water wheels were used to extract mechanical work from rivers to perform a variety of tasks much more efficiently than could be done by hand, such as crushing grain, spinning pottery wheels, or operating machinery in textile mills. With the invention of the electric generator in the late nineteenth century, it was not long before hydroelectric power established itself as a reliable and inexpensive method of power generation.

As technology has progressed over the last two centuries, the conventional method of generating hydroelectricity that has arisen involves creating a dam which obstructs the water's flow. As the water upstream continues to flow and hit the dam, the water level around the dam rises and creates an artificial lake where massive amounts of water builds up. The water at the bottom of this lake is now under high pressure due to the weight of all of the water above it, which creates an enormous amount of potential energy. By releasing some of the water at the bottom of the lake and forcing it through a turbine, this potential energy is converted into mechanical energy. This mechanical energy is converted into electrical power using a series of massive electric generators, which can then be distributed to the power grid with the help of transformers. A cross section of a typical hydroelectric power plant is shown in Figure 1.
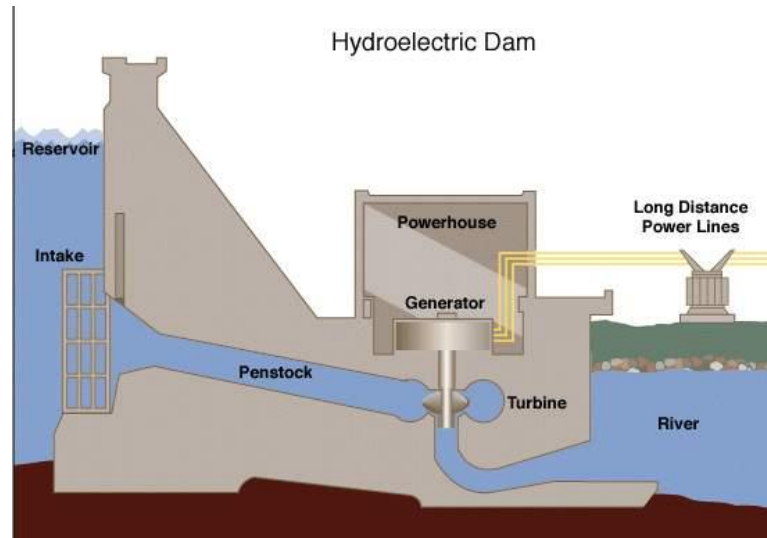
Figure 1: Cross section of a conventional hydroelectric power plant [1]

As of 2011, hydroelectric power produces 3.5 trillion kilowatt-hours of electricity annually (which represents 16% of global electricity generation), and almost all of this power is produced by the world's 45,000+ large hydroelectric dams. The total amount of power generated via hydroelectricity is expected to grow by an average of 3% annually, which it has averaged every year for the past four decades [2].

1.2   Motivation for Present Research

Conventional hydroelectric power has many advantages, the most notable of which is that it is a renewable energy, and one that has two orders of magnitude lower carbon footprint per kilowatt-hour than coal, oil, or natural gas [3]. Additionally, once the power station is already running, it is one of the cheapest forms of electricity, at 3 to 5 US cents per kilowatt-hour for plants that have over a 10 megawatt capacity [4].

One major feature of conventional hydropower is that it necessitates the creation of a large body of water to extract power from. Region-dependent, the lake that the dam

3

creates can be a popular tourist attraction and bring in a lot of revenue for the surrounding community. However, the creation of this lake also means that the natural habitat of many different forms of wildlife will be disrupted, which can involve preventing the migration of fish in the river as well as displacing any land-based animals (humans included) that might live along the river's shore. Another issue is that, often times, the ability of the hydroelectric plant to generate power can be compromised during long draught periods or, climate-dependent, during the wintertime, when the river flowing into the dam can freeze.

Dams and the lakes that they create also require substantial space, often taking up dozens of square miles of surface area and hundreds of thousands or even millions of cubic meters of water volume. But in some communities the biggest issue is that building a dam can be prohibitively expensive and take years of planning and construction time before any power can be generated. These properties can make conventional hydroelectric dams ill-suited to providing the power needs of certain groups of people, who are likely to turn to fossil fuels to fulfill their power needs even despite the presence of powerful rivers that flow through their communities. People living in areas that do fit this description, as well as any other organizations which could utilize highly mobile and quiet power generation create the potential market for a source of hydroelectric power that shares many of the benefits of conventional hydropower, but without severely disrupting the environment in which they are installed or requiring a long and expensive setup.

The most simple of such a device is the Hydrokinetic Turbine (HKT), which is capable of generating mechanical energy from a stream using only the kinetic energy that the moving water already has. This mechanical energy can then be used to make electrical power via a generator, similar to how wind turbines generate power from moving air.

Hydrokinetic Turbines can be classified into two main categories: vertical axis turbines and horizontal axis turbines. The difference between them is that, in horizontal axis turbines, the axis of rotation of the turbine is parallel with the flow direction, whereas in vertical-axis turbines the rotation axis of the turbines is perpendicular to the flow direction (usually such that the axis of rotation is in the same plane as the river's surface, or in a manner that is perpendicular to that surface). The different turbine types are shown in Figure 2 for Wind Turbines, although the concept is the same for Hydrokinetic Turbines.
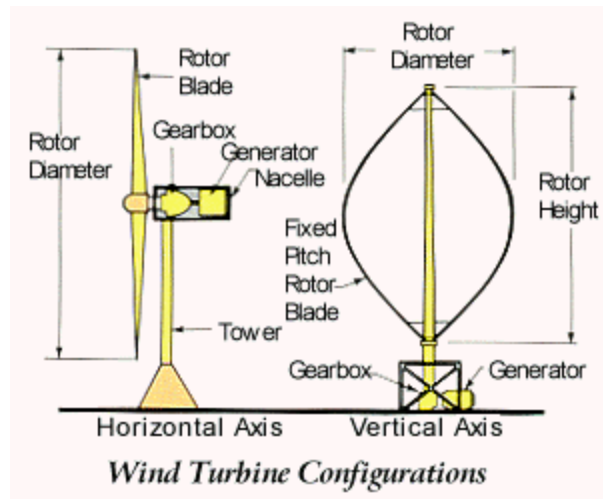
Figure 2: Horizontal Axis vs Vertical Axis Turbines [5]

1.3   Limits of Hydrokinetic Turbine Efficiency

Without having the luxury of utilizing a large static head, the total power output of hydrokinetic turbines can be expected to be much lower than that of conventional hydroelectric dams. To quantify the available energy for extraction, it is important to remember that the total rate of kinetic energy (KE) entering the turbine is given by

$$\dot{KE} = \frac{1}{2}\dot{m}V_i^2 \tag{1}$$

where $\dot{m}$ in this case is the mass flow rate into the turbine, and V_i is the velocity at the turbine inlet (which we can assume is equal to the free stream velocity). Keeping in mind that $\dot{m} = \rho A V_i$ then the flow of KE into the turbine is given by

$$\dot{KE} = \frac{1}{2}\rho A V_i^3 \tag{2}$$

where ρ is the density of the water, and A is the swept area of the turbine.

If all of this energy in the water were extracted, then the water at the turbine outlet would not be moving and therefore block the flow upstream. If this were the case, then this water would prevent the flow from entering the turbine and halt any future power generation. This means that the theoretical maximum power that can be generated by an ideal hydrokinetic turbine (i.e. a turbine with an infinite number of blades, no drag, zero hub diameter, and other unrealistic assumptions) is only a fraction of this total kinetic energy. This fraction is called the Ideal Turbine Power Coefficient (C_T) and is given by the equation

$$C_T = \frac{1}{2}\left(1 + \frac{V_o}{V_i}\right)\left(1 - \left(\frac{V_o}{V_i}\right)^2\right) \tag{3}$$

6

where V_i is the same as before and V_o is the velocity at the turbine outlet. This equation for the power coefficient is maximized at $\frac{V_o}{V_i}$= 1/3, which makes C_T= 16/27 $\cong$ 0.5926. This maximum is known as the Betz Limit and it makes the total power output for an ideal turbine given by

$$P_{ideal} = \frac{1}{2}\rho A V_i^3 C_T \qquad (4)$$

although the actual power one can expect to generate from a real turbine is still a good bit lower than this value [6].

It is also useful to talk about certain parameters in order to non-dimensionalize turbine geometry or velocity conditions, so that they can be more easily compared to other fluid researcher's results. The first parameter is the ratio of the speed at the tip of the turbine to the fluid speed, called the Tip Speed Ratio (TSR) and is given by:

$$TSR = \frac{R\Omega}{V_i} \qquad (5)$$

Where R is the turbine radius and Ω is the rotation rate (in radians per second). The tip speed ratio is useful for comparing turbine performance in different flow scenarios. The next parameter is the solidity ratio (σ) of the turbine, which is defined as the ratio of the chord length of the blade at the tip (c) divided by the turbine circumference ($2\pi R$) and then multiplied by the number of blades (B).

$$\sigma = \frac{Bc}{2\pi R} \qquad (6)$$

The solidity ratio is a geometric feature of the turbine itself, and it is one of the parameters that turbine designers must try to optimize for each flow scenario. The

dimensionless fluid velocity that is often used in similar studies is the Reynolds Number (Re), which is given by

$$Re_x = \frac{\rho V_i x}{\mu} \tag{7}$$

where x is some characteristic length of the system and μ is the dynamic viscosity of the fluid.

1.4 Introduction to Turbulence Modeling

For the past couple of decades, the issue of modeling the performance of rotating turbines was done with blade-element momentum (BEM) approximations. These methods use the angle of attack of the blades with respect to the incoming flow, the speed of the water coming into contact with the blades, the rotation rate of the blades, and other relatively simple geometric properties to find the resulting forces on a differential element of the blade. Integrating these quantities over the length of the blade and multiplying the result by the number of blades allows for the calculation of turbine power, thrust, and a few other useful quantities.

The BEM models are still in use today due to their reasonable accuracy and relative simplicity, but they fail to take into account many of the complexities of the flow around a hydrokinetic turbine. For instance, the BEM model assumes that the flow is largely 2D with respect to the blade surface, which means that it cannot take into account interaction between adjacent blade elements nor can it predict the effects of the vortex shedding at the blade tip, blade trailing edge, and turbine hub [7]. This vorticity affects how the incoming flow interacts with the blade and thus must also impact turbine

8

performance. Therefore, to find more accurate results using numerical methods, a way of taking these effects into account is needed.

To come up with a method of resolving these issues, it is important to remember that the motion of any Newtonian fluid is governed by the famous Navier-Stokes equations. The equations are derived from conservation of mass and momentum for a differential element of a Newtonian fluid, and whose form for incompressible flow with constant viscosity is expressed below in vector form.

$$\nabla \cdot \boldsymbol{v} = 0 \tag{8}$$

$$\rho \left(\frac{\partial \boldsymbol{v}}{\partial t} + \boldsymbol{v} \cdot \nabla \boldsymbol{v} \right) = -\nabla p + \mu \nabla^2 \boldsymbol{v} + \boldsymbol{f} \tag{9}$$

where ∇ is the vector differential operator, $\cdot$ represents the vector dot product, $\boldsymbol{v}$ is the velocity vector of the fluid, ρ is the fluid density (which through the incompressibility assumption is a constant), t is time, p is pressure, μ is the fluid's viscosity, and $\boldsymbol{f}$ is the net body force per unit volume vector.

Finding an analytical solution to the Navier-Stokes equations in an arbitrarily shaped domain with specific boundary and initial conditions remains one of the greatest challenges of modern mathematics [8]; even using direct numerical simulation to "brute force" a solution to the Navier-Stokes equations remains an impossibility for all but the simplest of flow scenarios [9]. However through the process of Reynolds decomposition, which breaks down each of the four unknowns of the Navier-stokes equations (the velocity in three-dimensions as well as the static pressure) into an average quantity and a fluctuating quantity, the resulting problem becomes more tractable. Keep in mind that this Reynolds-Average Navier-Stokes (RANS) process creates more unknowns than there

are equations to solve, so more equations must be found in order for the number of equations to match the number of unknowns. These equations that are introduced have to describe the flow in the best way at a minimal computational cost, and the entire field of RANS Turbulence Modeling has been dedicated to finding the equations which accomplish this goal the best.

Luckily, a great deal of research in turbulence modeling has already been done, but even so using RANS solvers to analyze designs for rotating turbines in 3D is a problem that until recently remained computationally unfeasible to solve. Recent advances in turbulence models (such as the k-ϵ model, k-ω model, and their more modern variations) retain relative computational simplicity yet are able to capture many complicated features of turbulent flows. Massive leaps in computing technology allow simulations with orders of magnitude more complexity than those that could be run just a decade ago, which means that using fully three-dimensional RANS analysis of a rotating turbine is well within the capacity of many modern high-end desktop computers.

1.5   Introduction to Computational Fluid Dynamics

Computational Fluid Dynamics (CFD) is a relatively new branch of fluid mechanics that utilizes numerical methods and powerful computers to find approximate solutions to complicated fluid flows. From these solutions important quantities which are relevant to the researcher or designer can be subsequently determined. CFD lets its practitioners model how their product or concept will interact with fluids in a way that is often much quicker, cheaper and more practical than building a prototype and conducting the relevant experiments.

The main motivation of applying CFD is modeling the behavior of turbulent flows, as virtually all flows of practical interest involve turbulence [10]. In order to do this, there are several steps that need to occur. First, the geometry of the simulation must be created using Computer-Aided Design (CAD) software such as AutoCAD, Solidworks, or, as was the case for this study, ANSYS DesignModeler (v13.0). Next, the domain needs to be discretized into many smaller, simply-shaped chunks called elements.

This is discretization is done by importing the CAD file into a meshing program, where the user can specify many various parameters to create a desirable mesh. This step is very important, as the accuracy of the approximate solution that a numerical simulation will generate is extremely dependent on the nature, quality and fineness of the mesh that is being used. Creating a mesh that is detailed enough to capture all relevant flow characteristics is essential for high-quality solutions, however there are naturally limitations that the available computing resources place on how fine of a mesh can be created.

After creating a satisfactory mesh, an appropriate turbulence model must be selected which performs well under the flow conditions that could be reasonably expected for the present simulation. From there, boundary conditions are applied to the walls of the domain (and, for the case of a time-dependent simulation, initial conditions must also be applied) which best represent the situation that is being modeled. Additionally for the present study, modeling the rotating turbine blades in a HKT require the creation of a rotating zone, where various approximations to account for this rotation must be done. Finally, an interface linking the rotating zone and the non-rotating zone

11

must be created in order to formalize the connectivity between these domains, as well as selecting a series of solvers which are capable of finding a converged solution in a reasonable amount of time.

After the simulation is run, the various quantities that are important for each simulation can be extracted. In order to be sure that the results are not significantly affected by the truncation errors inherent in all numerical methods, other simulations of varying grid sizes with the same geometry, turbulence model, and boundary conditions must be run to verify mesh independence or mesh convergence [11].

1.6   Opportunity for Present Research

Thus far, there has been in-depth CFD research in the wind turbine field, and as a result the relationship of many different input and design conditions to the important outputs is relatively well understood in this application. Likely due to comparably fewer opportunities for funding, these relationships in hydrokinetic turbines are arguably less well understood. And while many similar phenomena occur in hydrokinetic turbines as they do in wind turbines, it is disingenuous to assume that wild turbine theory and design practices can be directly applied to hydrokinetic turbines [6].

Horizontal-Axis Hydrokinetic Turbines (HAKHT) were chosen for this study due to their higher efficiency, which is a result of lower incidence loss due to more of the fluid hitting the turbine blades of HAHKT's at an optimal angle than comparable vertical-axis HKT's [12]. Due to the relatively low power output of a single HKT, it is a natural progression that multiple units will be needed to fulfill most customers' energy needs.

12

The issue of the optimal location to place these turbines relative to each-other then becomes apparent. It is intuitively clear (and can be shown via experimental evidence and using CFD tools) that these turbines should not be placed directly downstream of one-another, as trying to extract energy from fluid that has already had a large percentage of its energy extracted from it is not particularly wise. In fact, according to experimental studies done by [13], it takes 35 turbine diameters downstream of an axial HKT for the averaged longitudinal velocity to reach 97% of the turbine inflow averaged velocity. However, the problem of how far away perpendicular to the flow direction these turbines should be placed in order to maximize power output is not well understood.

The research in this paper is intended to analyze the effect that separation distance perpendicular to the flow direction has in a pair of horizontal axis hydrokinetic turbines using Reynolds-Average Navier-Stokes Computational Fluid Dynamics modeling.

2. Simulation Setup

2.1 Geometry Selection and Generation

The geometry of the two turbines used in this study was taken from [14], which has a turbine diameter of 21 inches (0.5334 m), a hub diameter of 2.5 inches (0.0635 m), hub length of 15 inches (0.381 m), a uniform blade thickness of 0.5 inches (0.0127 m), a "leading edge to trailing edge" of blade axial displacement of 5.8584 inches (0.1488 m), and two blades, with each blade spanning an angle of 142.3 degrees

with respect to the hub. A perspective view of one of these turbines and a view from the flow direction are shown in Figure 3 and Figure 4.
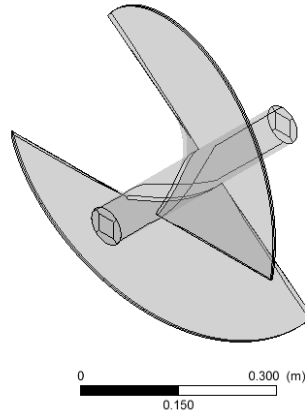

Figure 3: Perspective view of Turbine Geometry
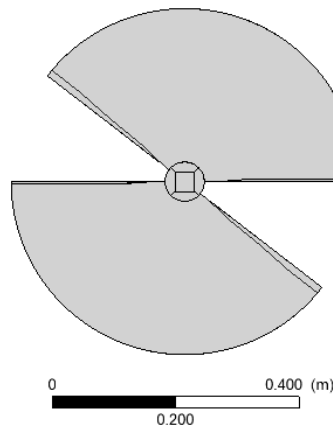
Figure 4: View of Turbine from Flow Direction

The turbine is designed to rotate at 150 RPM clockwise when viewed from the flow direction; this design was optimized to maximize the power generation on a relatively shallow (hence the small turbine diameter) yet fast-moving river with an average fluid speed of 2.25 m/s. These geometry and flow conditions make the TSR for these simulations equal to approximately 1.8619, while the solidity ratio is approximately 0.79055. However it is important to keep in mind that, for the purposes of this study, the

14

geometry of the turbines themselves is not as important as the separation distance between them.

To determine the effect that separation distance (d) has on turbine performance, several different river geometries must be created with different turbine separation distances in each one. The separation distance for the purposes of this paper is expressed as the distance between the axes of rotations of each of the turbines, as shown in Figure 5.
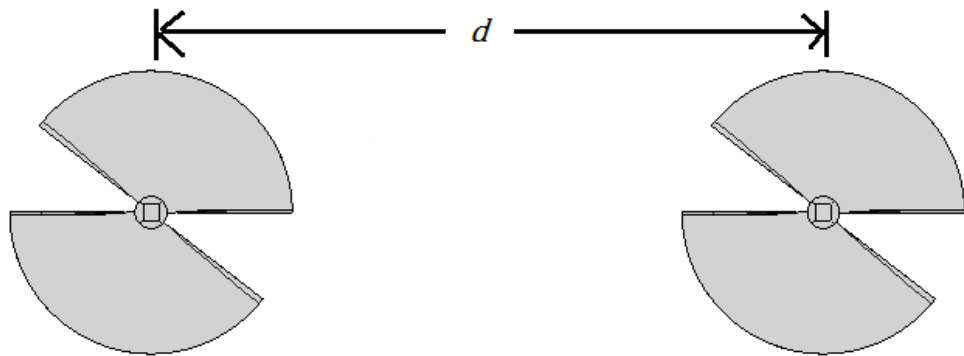

Figure 5: Definition of Separation Distance

Defining separation distance in this manner means that, with a turbine diameter of 21 inches, a separation distance of 21 inches means that the tips of the turbine blades will be just barely touching. With that definition in mind, five different geometries were created, with d equal to three, four, five, six and seven turbine radii (31.5 inches, 42 inches, 52.5 inches, 63 inches, and 73.5 inches respectively).

The computational domain that was constructed for all of these simulations is 30 feet (9.144 m) wide and 10 feet (3.048 m) tall. It is important in the geometry setup that the turbines are placed sufficiently far away from the river bed in order to prevent any wall effects from interfering with the results. This would also represent expected

15

operating conditions; as such a hydrokinetic turbine would need to be placed a far away from the river bed to maximize the energy of the water that is passing through the turbine as well as minimize the chances that the turbine is damaged by any heavy debris traveling along the river bed. As such, the turbines are placed 74 inches (1.8796 m) away from the bottom of the river bed, as well as 46 inches (1.1684 m) beneath the free surface of the water.

The computational domain in these types of simulations needs to be long enough so that the inlet and outlet pressure/gradient boundary conditions do not interfere with the true nature of the flow around the turbines. In order to meet this goal, the river geometry created for this study is 30 feet (9.144 m) in depth, with 10 feet (3.048 m) upstream and 20 feet (6.096 m) downstream of the turbine leading edge in order to capture the turbine's wake and thus the effect that that wake will have on turbine performance.

A very important but not often discussed part of the geometry generation in Hydrokinetic Turbine CFD simulations is how large the cylindrical rotating domain that encloses the turbines should be. It has been shown by [15] that a larger rotating domain radius more accurately reflects experimental results, however because the present study involves simulating two turbines that are close together instead of one, creating large rotating domains for these turbines is not possible. This is because the generation of a rotating domain with a large diameter in this scenario would cause the domains to intersect and create nonsensical results. Therefore the nature of the present simulations places a hard restriction on the allowable size of the rotating domain for the present study based upon their separation distance. Even further constraints on the rotating domain size

16

become apparent when attempting to mesh the river geometry and avoid the generation of high aspect ratio elements in between the rotating turbine domains.

With all of these constraints in mind, the radii of the rotating domains for this study are 1.25R (26.25 inches) for d= 3R, 1.5R (31.5 inches) for d= 4R, 1.75R (36.75 inches) for d= 5R, 2R (42 inches) for d = 6R, and 2R (42 inches) for d = 7R. The non-rotating river domain for the d =3R, d = 5R and d = 7R separation distances are shown in Figure 6a, Figure 6b, and Figure 6c.
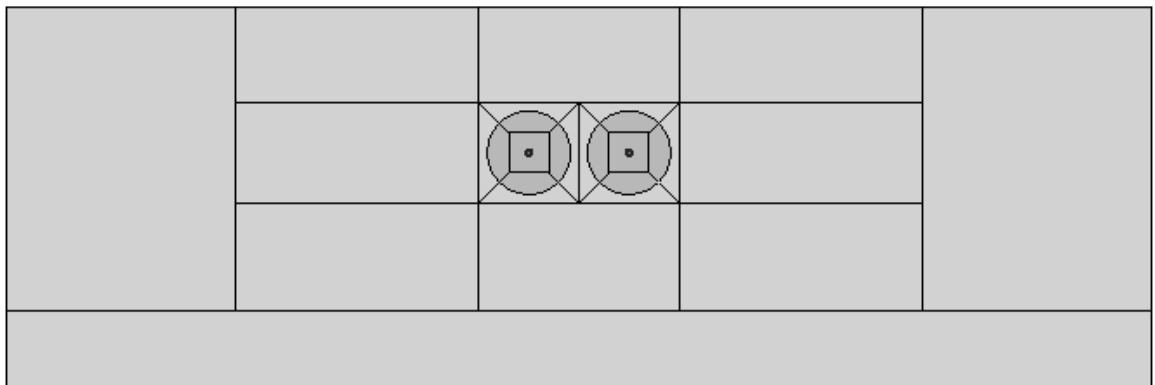
a)
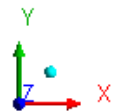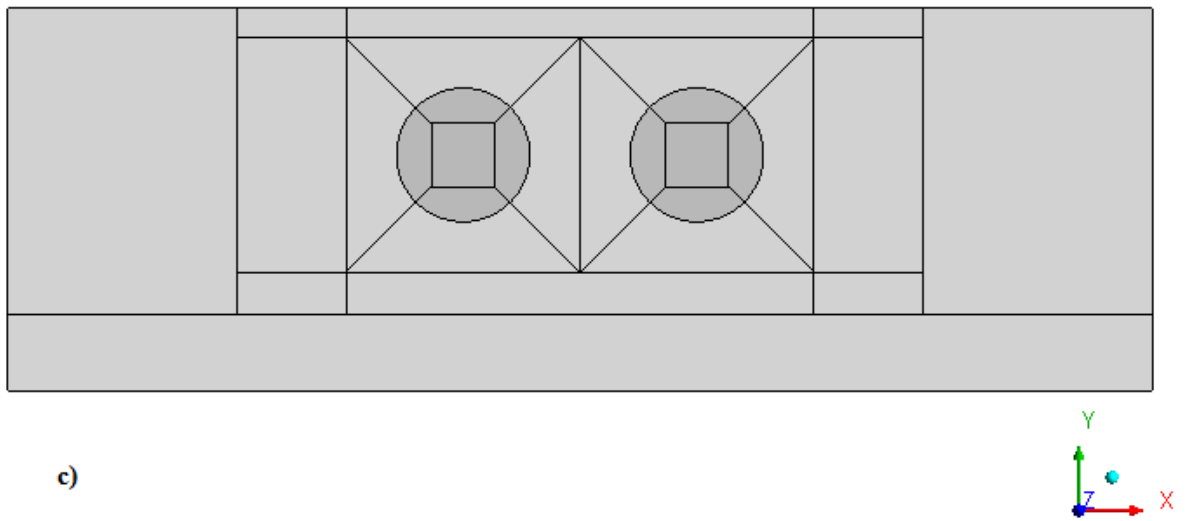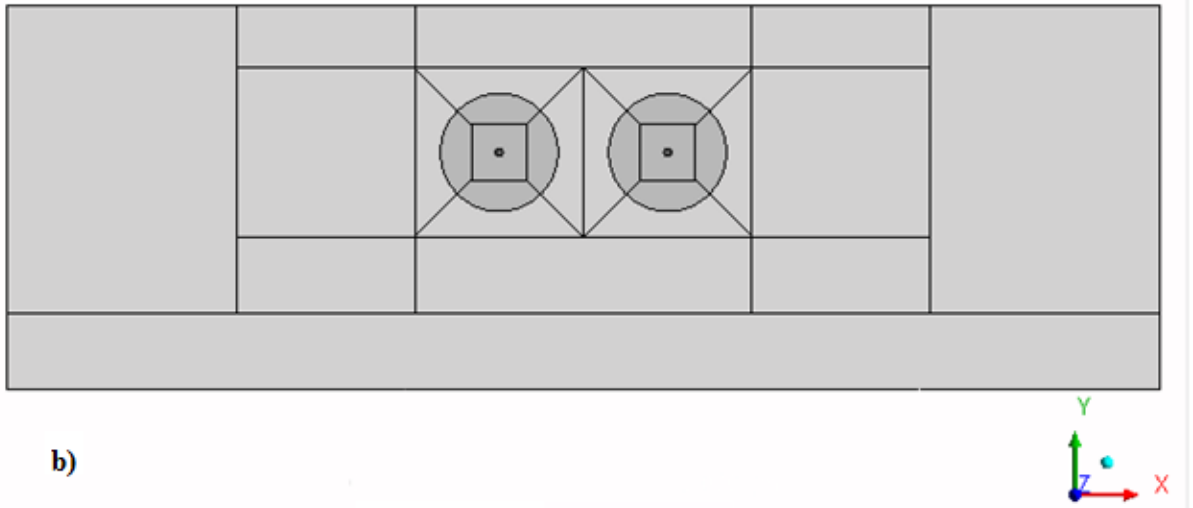
Figure 6: Front View of nonrotating domains for a) d = 3R, b) d = 5R, c) d = 7R

The entire assembled simulation domain (complete with rotating and non-rotating zones) for the 5r separation distance is shown in Figure 7 for a perspective view and Figure 8 for the view from the flow direction.

0   5.000 (m)

2.500
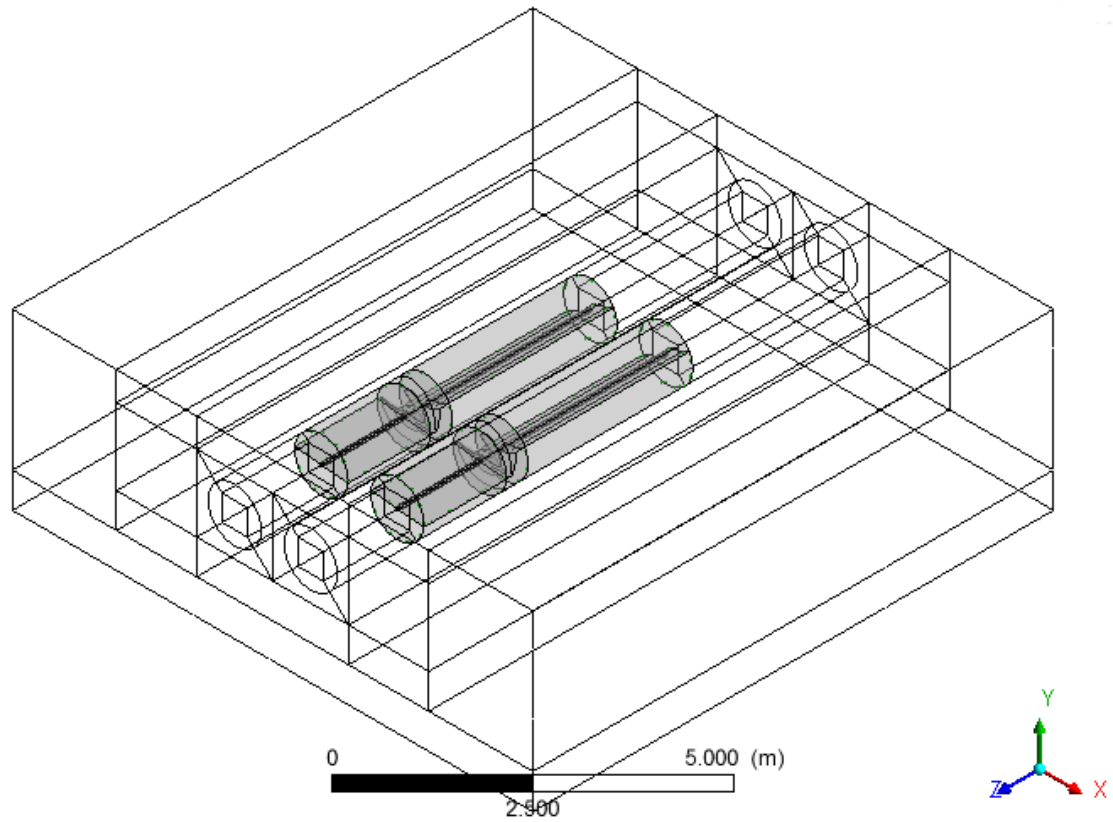
Figure 7: Perspective View of Simulation Space (d = 5R)

0   3.000 (m)

1.500
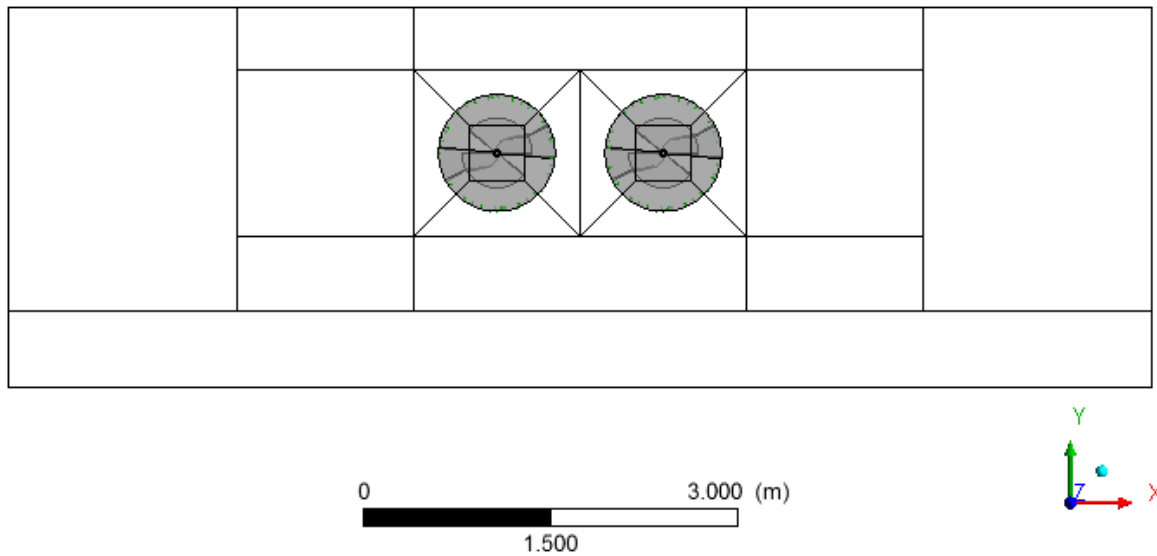
Figure 8: Inlet View of Simulation Space (d = 5R)

In both figures, the river region is shown with transparent faces, whereas the left and right turbine regions are shown at 75% transparency in order to highlight the boundaries of the different regions as well as show the locations of the turbines themselves.

For each simulation, the cylindrical rotating domains extend 60 inches (1.524 m) upstream and 126 inches (3.2004 m) downstream from the leading edge of the turbine blades.

2.2   Mesh Generation

The turbine domain geometry, turbine hub, and river geometries were all created and meshed separately and then combined in order to use different software to model each domain. The river domain and hub domains were solid modeled in a manner that makes each solid body in those regions have four sides. This procedure allowed for the creation of a structured hexahedral mesh throughout all domains, which has a number of advantages over the comparatively simpler to setup unstructured meshes that many other CFD practitioners use.

The use of a fully structured mesh allowed for the creation of elements with very high quality even in the region close to and surrounding the turbine blades; usually in these types of simulations a minimum meshing quality of above 0.30 is desired, but for all simulations in this computational study a minimum mesh quality of 0.40 was achieved. A similarly lofty goal of an aspect ratio below 4 for all elements was also achieved for all simulations. These outcomes are possible because the structured mesh creates a very well-organized geometry discretization on the blade surface (as seen in

Figure 9) as well as creates a smooth inflation layer from the surface of the blades to the free stream (as demonstrated in Figure 10), which is intended to capture the complex turbulent effects originating on the blade surface, blade leading edge and blade tips.
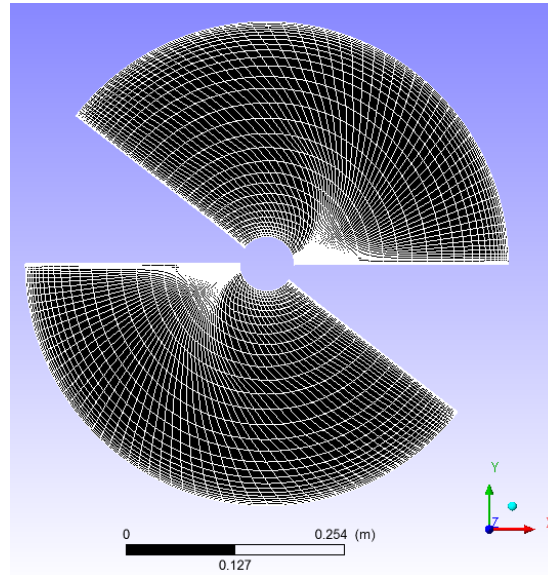
Figure 9: Blade Surface Mesh Viewed from Flow Direction (d = 5R)
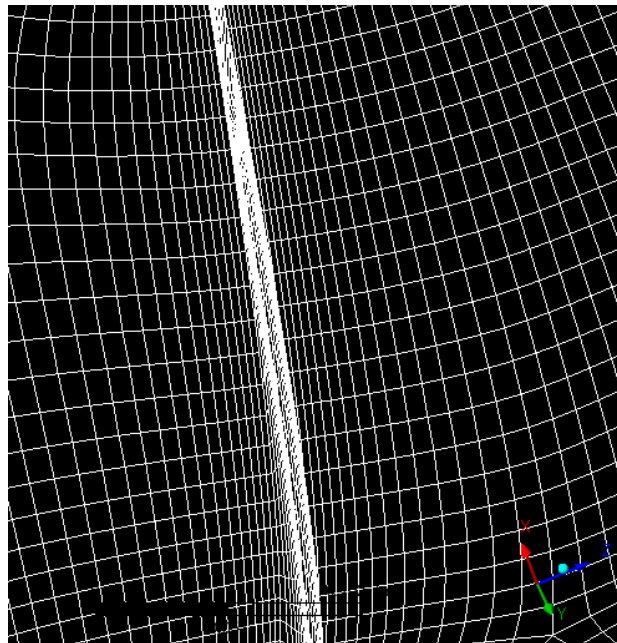
Figure 10: Mesh extending upstream and downstream of blade tip (d = 5R)

Another advantage to the fully structured nature of the mesh is that it allows for the creation of a river domain mesh that is symmetric about the midplane between the two turbines, which means that any differences in calculated performance between the left and right turbine cannot be attributed to meshing asymmetries.

In order to map the solution from one of these domains to the other, mesh interfaces that link each exterior surface in the turbine domains to its counterpart in the interior of the river domain must be created. Similar grid interfaces are used for the fluid upstream and downstream of the turbine hubs, as well as for the General Grid Interface (GGI) surrounding the turbine blades in each rotating domain.

For the d=3R, d=4R, and d=5R separation distances, two simulations with different mesh sizes were run in order to verify mesh independence of the results. These two mesh sizes are shown for the 5R separation distance in Figure 11 and Figure 12 as viewed from the inlet of the domain.
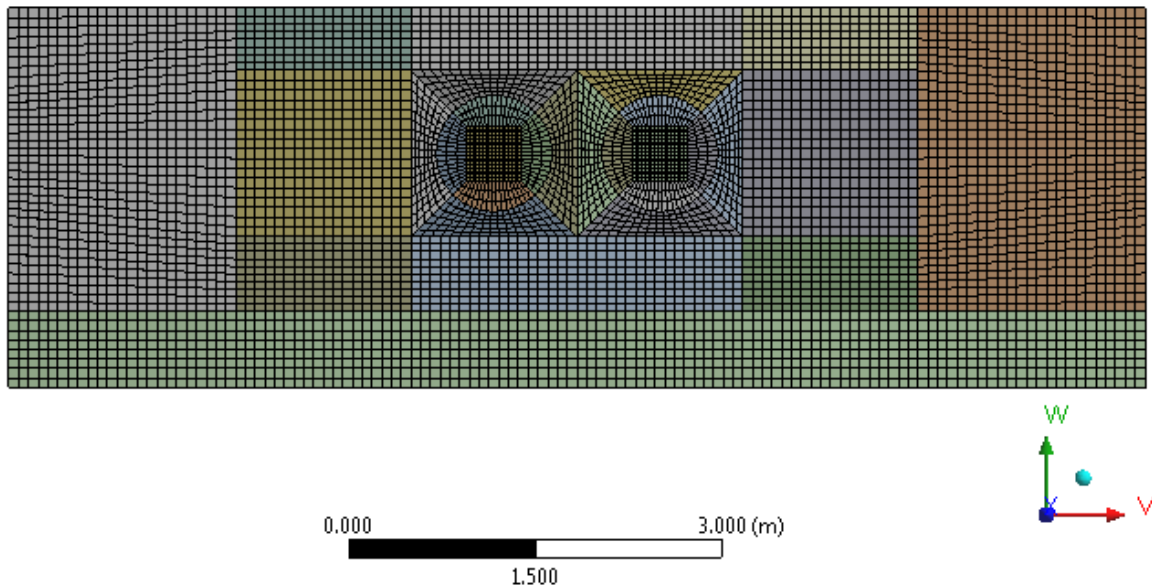
Figure 11: Coarse Mesh Front View (d = 5R)
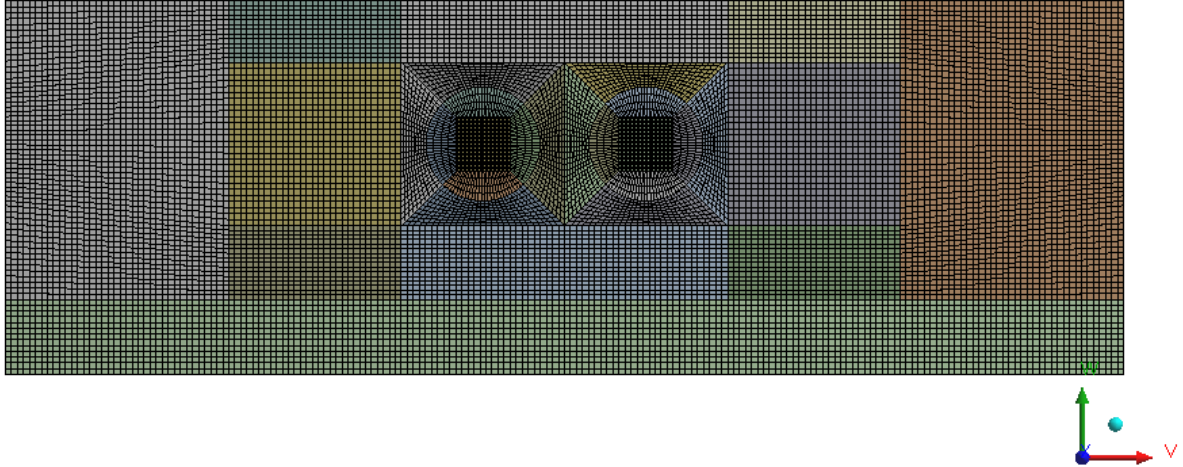
Figure 12: Fine Mesh Front View (d = 5R)

It is worth noting that there is no inflation layer in the mesh at the walls of the river bed; this was a conscious decision intended to reduce the number of elements involved in each simulation. This comes at the cost of not accurately representing the flow near walls of the simulation, but because the turbines are placed far enough away from the walls then that would not dramatically affect the calculated flow around the turbine nor calculated turbine performance.

For the coarse meshes at every separation distance, approximately 650 thousand structured elements were used to discretize the river domain, approximately 1 million elements each in both the rotating left and right turbine regions, as well as around 700 thousand elements to capture the upstream and downstream hub region of the river. For the fine meshes, approximately 2.6 million elements were used to discretize the river, 1.5 million elements each for the rotating domain around the left and right turbine, and 700 thousand elements for the upstream and downstream hub regions. Altogether, that makes approximately 3.5 million elements for each of the coarse mesh simulations and approximately 6.1 million elements for the fine mesh simulations.

23

The hub and river domains were meshed in hexahedral elements using ANSYS ICEM CFD's mapped face meshing feature, whereas the domains around the two turbines were meshed with hexahedral elements using the Turbogrid extension for ANSYS Workbench v13.0.

2.3   Approximations of Turbine Rotation

The nature of vortex shedding on solid bodies makes even a relatively simple flow, such as 2D flow past a cylinder, have an oscillatory solution. It should come as no surprise, then, that the flow past a rotating turbine (with a much more complicated geometry than a simple cylinder) will also have an innately unsteady resulting flow. The importance of incorporating this turbine rotation and inherent flow fluctuations in our numerical simulations becomes paramount.

One approach to taking these fluctuations into account is to run a fully transient simulation, where initial conditions are assumed, and from those initial conditions the solution moves forward in time, calculating the flow state at every time step. To describe the turbine rotation accurately, the time step that the simulation uses must be small in relation to the rotation rate of the turbines, and the mesh around both turbine regions must rotate a small increment after each time step. After enough time steps have been run so that the initial flow assumptions have been "dampened out" there is a periodic flow pattern that will result. From there, expected turbine performance is derived via time-averaging operations over all of the generated data files.

Although potentially able to find very accurate solutions, there are a few major downsides to the fully transient solution method that make it very unwieldy to use.

Firstly, the simulation needs to run for often times several thousand time steps or more, which means that it can take weeks of computation time for a single simulation. This method also generates a ton of data files as results, and storing all of that data can be a challenge of its own. It is possible to save the data files after a every "X" number of time steps to cut down on the quantity of data stored, but it is difficult to know *a priori* how big of a number "X" should be in order to capture all of the fluctuations in the flow.

As an alternative to modeling all of these turbulent variations directly, it is possible to average-out all of these fluctuating effects to get an approximate steady-state solution. The so-called rotating reference frame models do just that; instead of rotating the mesh for each turbine a small angle during every time step, the movement of the turbine is instead incorporated into the governing equations which are solved around the turbine regions. These modified Navier-Stokes equations shown below represent conservation of mass and momentum in a rotating domain for incompressible flow with constant viscosity.

$$\nabla \cdot \boldsymbol{v_r} = 0 \tag{10}$$

$$\rho\left(\frac{\partial \boldsymbol{v_r}}{\partial t} + \boldsymbol{v_r} \cdot \nabla \boldsymbol{v_r} + \boldsymbol{\Omega} \times (\boldsymbol{\Omega} \times \boldsymbol{r}) + 2\boldsymbol{\Omega} \times \boldsymbol{v_r}\right) = -\nabla p + \mu \nabla^2 \boldsymbol{v_r} \tag{11}$$

In these equations, $\boldsymbol{v_r}$ is the velocity vector in the rotating reference frame, $\boldsymbol{\Omega}$ is the vector of revolution of the rotating domain (where the direction of $\boldsymbol{\Omega}$ is the direction the axis of revolution of the rotating domain, and the magnitude of $\boldsymbol{\Omega}$ represents how quickly the domain is rotating), and $\boldsymbol{r}$ is the vectored distance from the origin of the moving frame to an arbitrary point in the rotating domain, $\times$ represents the vector cross product, while ∇, p, t , ρ, $\cdot$,and μ refer to the same quantities and operations as they do in the non-

rotating Navier-Stokes equations. The extra terms that result from this rotating reference frame formulation, namely the $\boldsymbol{\Omega} \times (\boldsymbol{\Omega} \times \boldsymbol{r})$ and $2\boldsymbol{\Omega} \times \boldsymbol{v_r}$ terms in the momentum equations, represent the inertial centrifugal and Coriolis forces, respectively [16].

The benefits to this steady-state approach over a fully transient simulation are numerous; firstly, because there is no time stepping when using the rotating reference frame approach, it has much friendlier computation times. The data is also much easier to store and interpret, because the output of these simulations is often a single data file from which all important turbine performance parameters can be derived. Although strictly speaking not as accurate as the fully transient simulations, the rotating reference frame approximations are used in the vast majority of wind and hydrokinetic turbine CFD studies because of these benefits (and because most of the time the results of the transient and steady-state simulations end up being very similar anyways).

This study utilized the steady-state, rotating reference frame approach for all separation distances and both mesh sizes.

2.4   Turbulence Model Selection

As stated in the introduction, a turbulence model that accurately describes the flow conditions of our present situation must be selected. The model used for this study is the k-ω Shear-Stress Transport (SST) Model, developed by Menter [17] in 1994, due to its good behavior describing separating flows and flows with an adverse pressure gradient. This model is a combination of the k-ω model, which does well modeling turbulence at regions close to the walls, and the k-ϵ model, which better models free-stream turbulent behavior.

26

The k-ϵ and k-ω models have been used heavily in the turbulence modeling and CFD communities to great success; both models use two differential equations to keep track of the properties of the turbulent flow, making them fall under a more general category of two-equation turbulence models. The k-ϵ model keeps track of the Specific Turbulent Kinetic Energy (k) and the Specific Turbulent Dissipation (ϵ), which are defined using Einstein summation notation below.

$$k = \frac{1}{2}\overline{u_i' u_i'} \tag{12}$$

$$\epsilon = \nu \overline{\frac{\partial u_i'}{\partial x_k}\frac{\partial u_i'}{\partial x_k}} \tag{13}$$

In the above equations, u_i' represents the fluctuating portion of the Reynolds decomposition of u_i (which is itself a component of the velocity vector $\boldsymbol{v}$), ν is the kinematic viscosity of the fluid (given by μ/ρ), x_k is one of the three components of the direction vector, and the bar over certain quantities represents a time-averaging operation.

In a physical sense, k represents the kinetic energy of the turbulent fluctuations per unit mass (and hence has the units of (length)^2/(time)^2). ϵ in this model represents the rate at which the turbulence kinetic energy is converted into thermal energy (and has units of (length)^2/(time)^3); or, an alternative way of thinking about this quantity is that it is equal to the mean rate at which work is done by the fluctuating component of the strain rate against the fluctuating viscous stresses [10].

The k-ω model uses the same definition for the turbulent kinetic energy, but no longer explicitly solves for ϵ, instead choosing to utilize differential equations for the Specific Dissipation rate (ω) of the turbulent flow. The quantity ω does not have a strict

physical meaning, as it was derived entirely through dimensional analysis, but it can be thought of as the mean frequency of the turbulence (as it has units of 1/(time)). ω is often defined implicitly using the simple relationship

$$\omega = \frac{\epsilon}{k\beta^*} \tag{14}$$

where ϵ and k are the same as before, and β^* is a dimensionless constant that depends on the model being used.

The k-ω SST model utilizes blending functions to transition from the k-ω model close to the walls into the k-ϵ model in the free stream; this approach avoids the downsides of either model at a comparatively small computational cost. These equations, shown below in their most general form using Einstein summation notation, are coupled differential equations with (as you might expect from the name of the model) k and ω as the unknowns.

$$\frac{\partial(\rho k)}{\partial t} + \frac{\partial(\rho u_j k)}{\partial x_j} = \tau_{ij}\frac{\partial u_i}{\partial x_j} - \beta^*\rho\omega k + \frac{\partial}{\partial x_j}\left[(\mu + \sigma_k\mu_t)\frac{\partial k}{\partial x_j}\right] \tag{15}$$

$$\frac{\partial(\rho\omega)}{\partial t} + \frac{\partial(\rho u_j\omega)}{\partial x_j} = \frac{\rho\gamma}{\mu_t}\tau_{ij}\frac{\partial u_i}{\partial x_j} - \beta\rho\omega^2 + \frac{\partial}{\partial x_j}\left[(\mu + \sigma_\omega\mu_t)\frac{\partial\omega}{\partial x_j}\right]\dots \\ + 2(1 - F_1)\frac{\rho\sigma_{\omega 2}}{\omega}\frac{\partial k}{\partial x_j}\frac{\partial\omega}{\partial x_j} \tag{16}$$

These are the two differential equations that need to be solved in the k-ω SST model, but in these equations there are a plethora of constants and plenty of shorthand notations. The explicit definitions of these quantities are shown below.

$$\tau_{ij} = \mu_t \left(\frac{\partial u_i}{\partial x_j} + \frac{\partial u_j}{\partial x_i} - \frac{2}{3} \frac{\partial u_k}{\partial x_k} \delta_{ij} \right) - \frac{2}{3} \rho k \delta_{ij} \qquad (17)$$

$$\mu_t = \frac{\rho a_1 k}{\max(a_1 \omega; F_2 \Omega^*)} \qquad (18)$$

$$F_1 = \tanh \left(\min \left[\max \left(\frac{\sqrt{k}}{\beta^* \omega y}; \frac{500\nu}{y^2 \omega} \right); \frac{4\rho \sigma_{\omega 2} k}{CD_{k\omega} y^2} \right]^4 \right) \qquad (19)$$

$$F_2 = \tanh \left(\max \left[2 \frac{\sqrt{k}}{\beta^* \omega y}; \frac{500\nu}{y^2 \omega} \right]^2 \right) \qquad (20)$$

$$CD_{k\omega} = \max \left(\frac{2\rho \sigma_{\omega 2}}{\omega} \frac{\partial k}{\partial x_j} \frac{\partial \omega}{\partial x_j}; 10^{-20} \right) \qquad (21)$$

In the above relationships, τ_{ij} represents the Reynold's Stress Tensor (the k-ω SST model uses the Boussinesq eddy-viscosity Approximation to make this quantity a product of the eddy viscosity and the mean strain-rate tensor, therefore adding closure to the RANS equations [10]), δ_{ij} is the Kronecker delta function ($\delta_{ij} = 1$ if i = j, and $\delta_{ij} = 0$ if i ≠ j), μ_t is the turbulent dynamic viscosity, F_1 and F_2 are blending functions, $CD_{k\omega}$ is the positive portion of the Cross Diffusion term of Equation (16), y is the distance in the domain away from any solid surfaces, Ω^* is the absolute value of the vorticity, and β^*, σ_k, γ, β, σ_ω, a_1, and $\sigma_{\omega 2}$ are all model constants.

It is important to remember that the value of many of the constants shown in the above equations actually dependent upon the distance in the domain away from solid surfaces (y) as well as on the values of values of k, ω, and their spatial derivatives that the equations (15) and (16) are being evaluated at. The blending functions that take these

factors into account are what make the k-ω SST model distinct in comparison to most other two-equation models.

The value of these constants change according to the following relationship:

$$\phi = F_1 \phi_1 + (1 - F_1)\phi_2 \tag{22}$$

where F_1 represents the same blending function as before, ϕ represents the value of one of the constants that is used in the above equations (i.e. either σ_ω, σ_k, γ, or β), while ϕ_1 and ϕ_2 are given by the following set of values:

ϕ_1: $\quad \sigma_{k1} = 0.85 \quad \sigma_{\omega1} = 0.5 \quad\quad \beta_1 = 0.0750 \quad\quad \gamma_1 = \beta_1/\beta^* - \sigma_{\omega1}\kappa^2/\sqrt{\beta^*}$

ϕ_2: $\quad \sigma_{k2} = 1.0 \quad\quad \sigma_{\omega2} = 0.856 \quad \beta_2 = 0.0828 \quad\quad \gamma_2 = \beta_2/\beta^* - \sigma_{\omega2}\kappa^2/\sqrt{\beta^*}$

The constants that do not change based upon the value of F_1 are

$$\beta^* = 0.09 \quad \kappa = 0.41 \quad a_1 = 0.31$$

2.5   Boundary and Initial Conditions

The after selecting the turbulence model, the final step of the simulation setup is defining our boundary conditions and (in the case of the fully transient simulation) initial conditions. The boundary conditions must specify a value or a gradient of that value for all quantities that are to be found inside of that boundary. Put more explicitly: the value of the velocity in three dimensions, the pressure, the turbulent kinetic energy and the turbulent frequency (or a gradient of those quantities) at all boundaries in the computational domain must be found before any meaningful simulations can be run.

When looking at the river domain from the flow direction, the domain can be thought of as a "box." The left, right and bottom of the box just represent the river bed, so

30

these surfaces are given the simple boundary conditions that the velocity is zero and that the pressure gradient perpendicular to these walls are also zero. The top of this box represents the surface of the river, which is safe to assume has zero shear stress. This zero shear stress assumption means that the gradient of the velocity and gradient of the pressure normal to this so-called free surface (or symmetry boundary condition) are both zero.

The front of the river domain is given a uniform inlet velocity normal to that surface, U, of 2.25 m/s, while the pressure is assumed to be at a zero gradient here as well. In reality, rivers do not have a uniform velocity distribution throughout a cross-section of flow, but for the purposes of these simulations generating a uniform velocity distribution at the inlet guarantees that the flow entering both turbines will be the same flow that the turbine was optimized for. Additionally, uniform flow ensures that the same kinetic energy is entering both turbines, which means that any difference in power output between the left and right turbines cannot be attributed to variations in flow conditions surrounding each turbine. In fact, because the turbines are placed sufficiently far away from the walls of the simulation, U is also the velocity that can be assumed to be entering the turbine. The exit of the river domain (which is the "back" of the computational box) is a pressure outlet condition set equal to zero, and the velocity is assumed to be a zero gradient (which means that the turbulent flow has stopped developing downstream).

The boundary conditions for the two turbines themselves are both moving walls, which means that the velocity is specified and the pressure gradient normal to the turbine surface is zero. In our steady state simulations, the velocity of the walls of the turbine in

the stationary frame is given by $\boldsymbol{\Omega} \times \boldsymbol{r}$, but it is important to remember that the domain surrounding both turbines utilizes the rotating reference frame approach. In the frame of reference for the rotating turbine the walls of that turbine are stationary; thus relative to their respective rotating frames the velocity on the surface of each turbine is zero in the steady-state simulations. This zero-velocity boundary condition is also true for a transient simulation, as the velocity of the turbine blades with respect to the rotating mesh is still zero.

The boundary conditions for k and ω in the k-ω SST model are more complicated to determine, at least in comparison to the ones for the pressure and velocity. As might be expected from a symmetry boundary condition, the gradient of k and ω at the free surface is zero. However, for both the inlet and the outlet, the turbulent kinetic energy and specific dissipation rate boundary conditions are given by the following relationships:

$$k_{io} = \frac{3}{2} (U\,I)^2 \qquad \omega_{io} = \frac{\sqrt{k_{io}}}{l} (\beta^*)^{\frac{-1}{4}} \qquad\qquad (23)$$

Where k_{io} and ω_{io} are the values of the turbulent kinetic energy and turbulent frequency, respectively, at the inlet and outlet, I is the Turbulent Intensity, l is the Turbulent Length Scale, and U and β^* are the same as before [18].

It therefore becomes necessary to determine what, exactly the turbulent intensity and turbulent length scales are for this simulation. The turbulent intensity is defined as the ratio of the magnitude of fluctuating component of the flow to the magnitude of the steady component of the flow. The value of I at the inlet and outlet is calculated using the formula for a fully developed flow in a duct, which is given by

$$I = 0.16 \, Re_{D_h}^{-1/8} \tag{24}$$

where Re_{D_h} is the Reynold's number of the flow based upon the Hydraulic Diameter (D_h) of the duct [19]. Using the formula that the hydraulic diameter is equal to four times the duct area divided by the wetted perimeter, it can be easily found that for this river geometry $D_h = 7.3152$ m. Remembering Equation (7) for the Reynolds number and using the properties of water at 20°C, Re_{D_h} is found to be $1.638 \cdot 10^7$. Plugging this in to Equation (24), the Turbulent Intensity at the Inlet and Outlet is found to be 0.02006 for all simulations.

The turbulent length scale (l) for fully developed pipe flow is given by

$$l = 0.07 \, D_h \tag{25}$$

so using the hydraulic diameter of the river geometry it is found that $l = 0.51206$ m [20]. Now that the turbulent intensity and turbulent length scales are known, the values of k_{io} and ω_{io} can be determined, although these values are calculated automatically in FLUENT and are not important parameters for the purpose of this study.

In a similar fashion, the values of k and ω at the solid walls of the domain (which in our simulations refers to the river bed and the turbine blades) are given by the following relationships:

$$k_{wall} = 0 \qquad \omega_{wall} = 10 \frac{6\nu}{\beta_1 (\Delta y_1)^2} \tag{26}$$

where ν is the kinematic viscosity, β_1 is a constant, and Δy_1 is the distance to the next point away from the wall [17].

For a transient simulation, the "zeroth" time step is usually initialized based upon the steady state solution. As the solution moves forward in time, the time-dependent features of the flow will start to manifest themselves in the simulation. In order to allow time for this to occur, it has become common practice in transient CFD simulations to discard the data from the first several turbine revolutions before any post-processing operations are performed.

2.7   Solver Selection

The last bit of information that must be specified before any simulation can be run are the solvers that FLUENT will use in order to find the best numerical solution for the discretized geometry, boundary conditions, governing equations, and surface interfaces that it is given. Namely the Pressure-Velocity Coupling, Time Stepping and Spatial Discretization Schemes must ideally be chosen in a way that lets the solution converge as rapidly and with as much accuracy as possible.

With those objectives in mind, the "Coupled" scheme was used for the Pressure-Velocity coupling, while the "least squares cell based" and "standard" schemes were used for the gradient and pressure solvers, respectively. For the momentum, turbulent kinetic energy, and specific dissipation rate equations, a "second order upwind" scheme was selected. Although all simulations in this study were steady state, a "Pseudo-Transient" time step option was utilized. More information about how each of these solvers work as well as their advantages and drawbacks can be found in the *FLUENT 14.0 User's Guide* [22].

3. Simulation Quality and Results

3.1 Turbine Performance Metrics

When attempting to optimize turbine performance, it is necessary to define which parameter(s) of the turbine should be optimized. For the purposes of this study, the separation distance that maximizes the total power that the turbine is generating needs to be discovered. Or, if such a distance is found not to exist, then the objective would be to find a correlation between the separation distance and the power output.

Power is not the only important output parameter; naturally, the turbine drag force will want to be minimized in order to reduce the strain on the supports that hold the turbines in place. The drag force can be thought of as the "cost" that generating power has on the mechanical and electrical machinery used to create that power. Thus, minimizing that drag force will correlate with an increase in the lifespan of the equipment used; therefore, a similar relationship between resultant drag forces and separation distance would also be very valuable.

It is also useful to nondimensionalize both the drag and the power output, so that other CFD practitioners can more readily compare their results to these. The coefficient of drag (C_D) and coefficient of performance (C_p) do just that and are, respectively, defined according to the following relationships

$$C_D = \frac{F_D}{\frac{1}{2}\rho U^2 A} \tag{27}$$

$$C_p = \frac{P}{\frac{1}{2}\rho U^2 A \Omega} \tag{28}$$

where F_D is the resultant drag force and P is the resultant power output from one of the turbines in the simulations.

The objective of these CFD simulations are to discover the relationship between the separation distance of the turbines and the coefficient of performance and coefficient of drag from both turbines.

3.2   Turbine Performance Outputs

After running the simulations as described above, the following relationships between turbine power vs separation distance were observed as shown in figure 13.
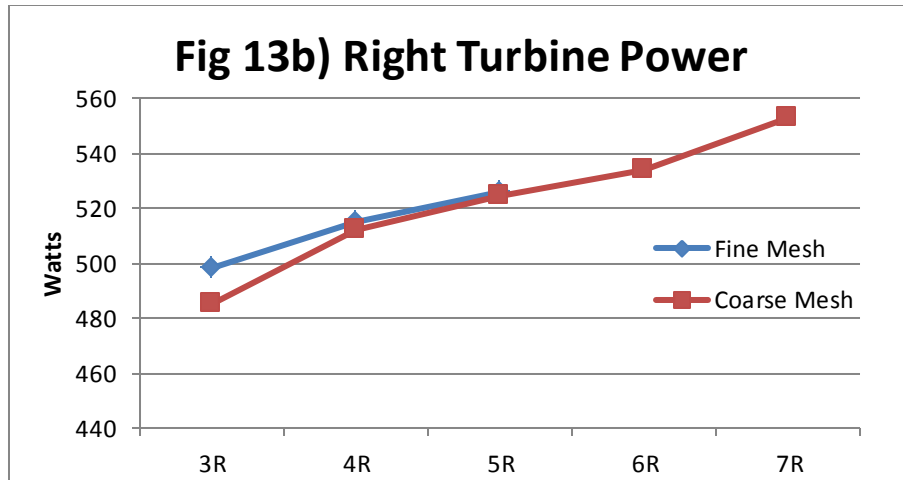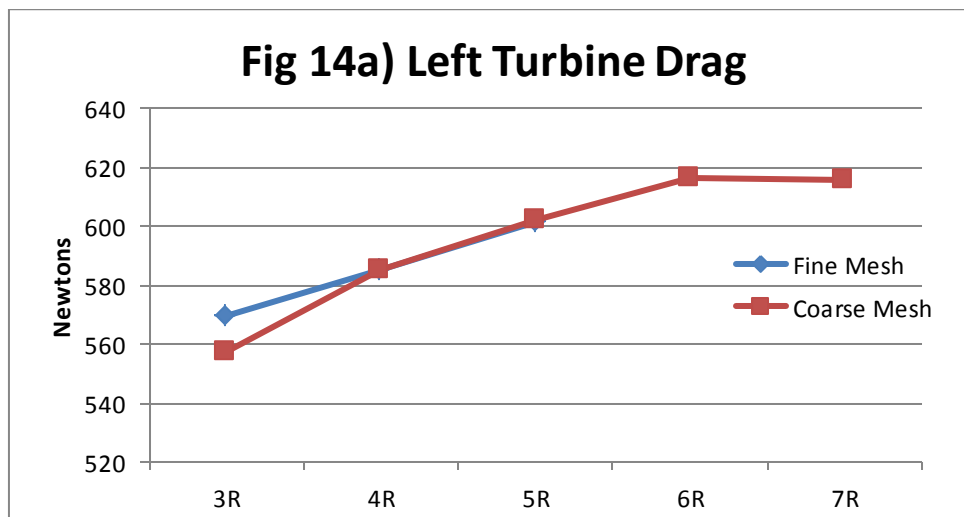

Fig 13a) Left Turbine Power
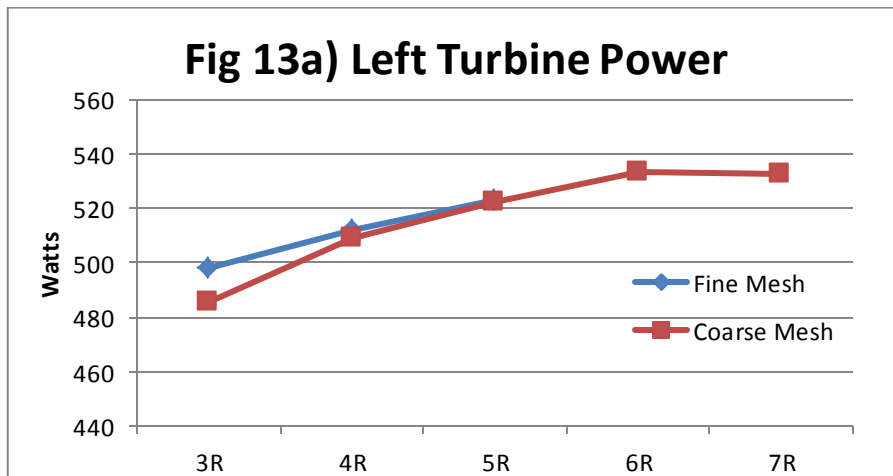
Figure 13: a) Left Turbine Power vs Separation distance b) Right Turbine Power vs Separation Distance

The turbine drag vs separation distance graph obeyed a similar relationship, as shown in figure 14.
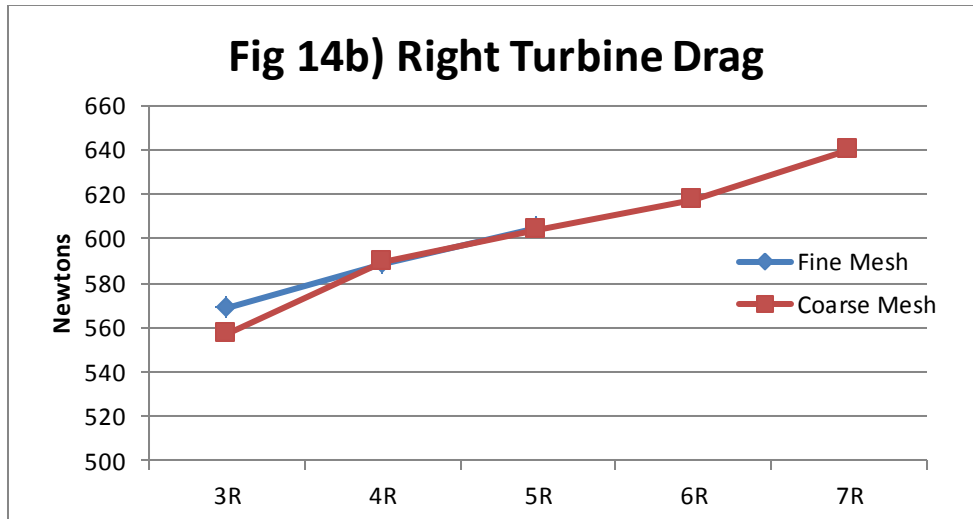
Figure 14: a) Left Turbine Drag vs Separation Distance b) Right Turbine Drag vs Separation Distance

It is worth mentioning that the simulation for the d=7R geometry was unable to be meshed to the same quality as the other simulations in this study. This is for two separate reasons. The first is an artificial limitation of twice the turbine radius that Turbogrid places on how large the rotating domain can be in relation to the turbine; this means that the rotating domain size to separation distance ratio is smaller for the d=7R simulation than it was for the other simulations in this study. The other limitation has to do with how the mesh is structured which forces high aspect ratio elements upstream of the rotating domain inlet and downstream of the rotating domain outlet. These two factors help to explain why the drag and power outputs for the d=7R separation distance do not match up as neatly with the results of the other simulations.

It is also valuable to look at the percent difference between the left turbine and the right turbine power when separation distance is held constant. Doing this in figure 15, the following relationship is observed.

38

	Mesh	d=3R	d=4R	d=5R	d=6R	d=7R	Units
% Power Difference	Fine	0.032311	0.53658	-0.56709	-	-	%
	Coarse	-0.02081	-0.5715	-0.14763	-0.14678	-3.85579	%

Figure 15: Percentage different between left Turbine and Right Turbine power

A positive value of this quantity indicates that the left turbine is generating that much more power than the right, whereas a negative value would represent that the right turbine is generating more power than the left.

From these figures, we can see three very important relationships:

1) Holding separation distance constant, there seems to be a negligible difference in both resultant drag and power output between the left turbine and the right turbine. This is good news for customers who are looking to apply this research, because that means that the left generator and the right generator will be subject to approximately identical power loads, and will thus "wear out" at the same rates.

2) The Turbine Power and Drag both appear to asymptotically approach a constant value when they are brought further and further apart. One could intuitively guess that the turbines will cease interacting if they are brought infinitely far apart, so these results do make sense.

3) Both the left and the right turbine appear to generate in the order of 10% less power and 10% less drag when the turbines are close together in comparison to when they are far apart. This suggests that, in order to maximize the power output of these turbines when placed in a uniform flow field, the turbines should be separated as far away as possible.

Expanding on the third point: The rivers in which these turbines will be placed are, in general, not uniform flow fields. When this is the case, all turbines should be placed in an area of the flow that maximizes the kinetic energy of the water that will be entering those turbines. However, even in non-uniform flow conditions there will still exist a large, fast-moving region of the flow that will have an almost uniform flow distribution (i.e. the gradient of the velocity field will be near zero). The results of this study suggest that the turbines should be placed far apart from each other within that high-velocity region.

3.3   Simulation Quality Metrics

In order to ensure that the results of the CFD simulations that were generated by this study are representative of reality, three different approaches were utilized to verify simulation accuracy.

The first method of investigating the accuracy of the simulations involves plugging in the results (for static pressure, the three velocities, and k and omega) that are obtained numerically back into the governing equations that are being solved in the first place. Because there are six governing equations (one for continuity, x-momentum, y-momentum, z-momentum, k and ω), then six so-called "Residuals" are generated after every iteration. Each residual can be thought of as a "grade" for how well the results satisfy the given differential equation after it has been discretized by the mesh, with a better grade corresponding to lower residual values. For a steady-state simulation, the residuals start off near 1 and quickly drop down and eventually level off and fluctuate around a certain value after several hundred to a few thousand iterations; the value that the residuals fluctuation around is known as the converged residual. For the steady-state

simulations, the solution is generally not considered converged until all of the converged residuals fall below a certain value. For a transient simulation, a maximum number of iterations per time step as well as minimum residual criteria are specified; the simulation moves forward a time step after either of these two conditions are satisfied.

The second method of verifying numerical accuracy is by looking at the pressure, velocity, turbulent kinetic energy, specific dissipation rate, and other contours of the flow solution. When viewing the contours of these quantities using planes to get 2D slices of the results, there should not exist many "sharp" edges on the contours (i.e. they should be relatively smooth). If the contours show these sharp edges in an area where it would not make sense for these edges to exist in reality, then it is likely that the mesh is not accurately capturing the complicated flow conditions in that area. It is entirely possible that a solution is found which satisfies the discretized governing differential equations very well (and would therefore have a low residual), but because the mesh could discretize the domain in a manner that does not capture all characteristics of the flow, that simulation could still generate results which do not optimally reflect reality. Viewing these slices of the flow to discover if this is the case is a simple yet valuable tool for any CFD practitioner, and if the discretization is found to not represent the flow very well, then the mesh needs to be refined in that area and the simulation re-run. This method of investigating the solution quality is a "dummy check" in the sense that there are no quantities that are being measured, which makes this a subjective and purely qualitative method of determining how confident a researcher should be in their results.

The third and final method of verifying the solution quality that this study uses is through the calculation of a quantity known as the dimensionless wall distance (y^+), which is given by

$$y^+ = \frac{u_* y}{\nu}$$ (29)

In this equation, u_* is the friction velocity (which is given by $u_* = \sqrt{\tau_w / \rho}$, where τ_w is the wall shear stress and ρ is the fluid density), y is the distance to the nearest solid wall, and ν is the kinematic viscosity, as before [21]. This is a quantity that can only be found after the solution is calculated, and can also be used to determine the applicability of the mesh that was used to the capabilities of the model that was used. For the k-ω SST model, the y^+ value at the wall should be either less than 3 (which would represent when the mesh itself is taking into account the turbulent effects) or between 30 and 300 (which would represent when the k-ω SST model is taking these effects into account) [17][10].

3.4   Simulation Quality

From looking at the figures 13 and 14 from Section 3.2, there appears to be good agreement in turbine outputs between the coarse mesh and the fine mesh, especially when the separation distance is increased. Additionally, the velocity contours, blade pressure contours, and surfaces of constant vorticity have good agreement between the fine meshes and the coarse meshes as seen in Figures 16, 17, and 18 for the d=5R separation distance.
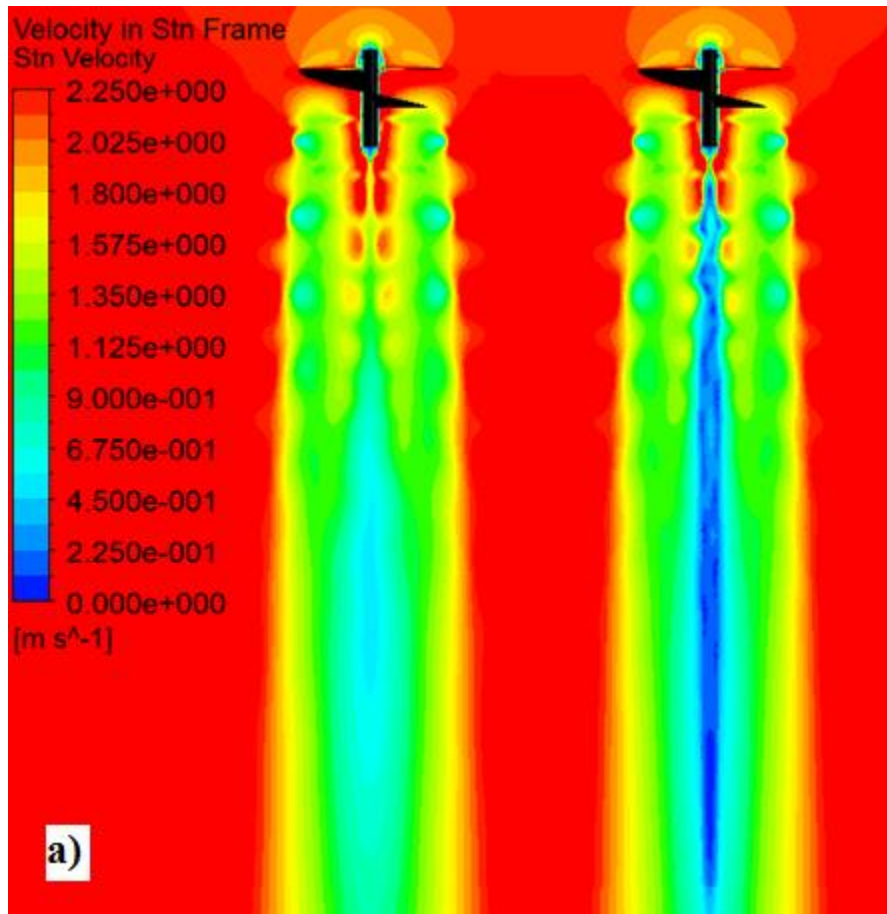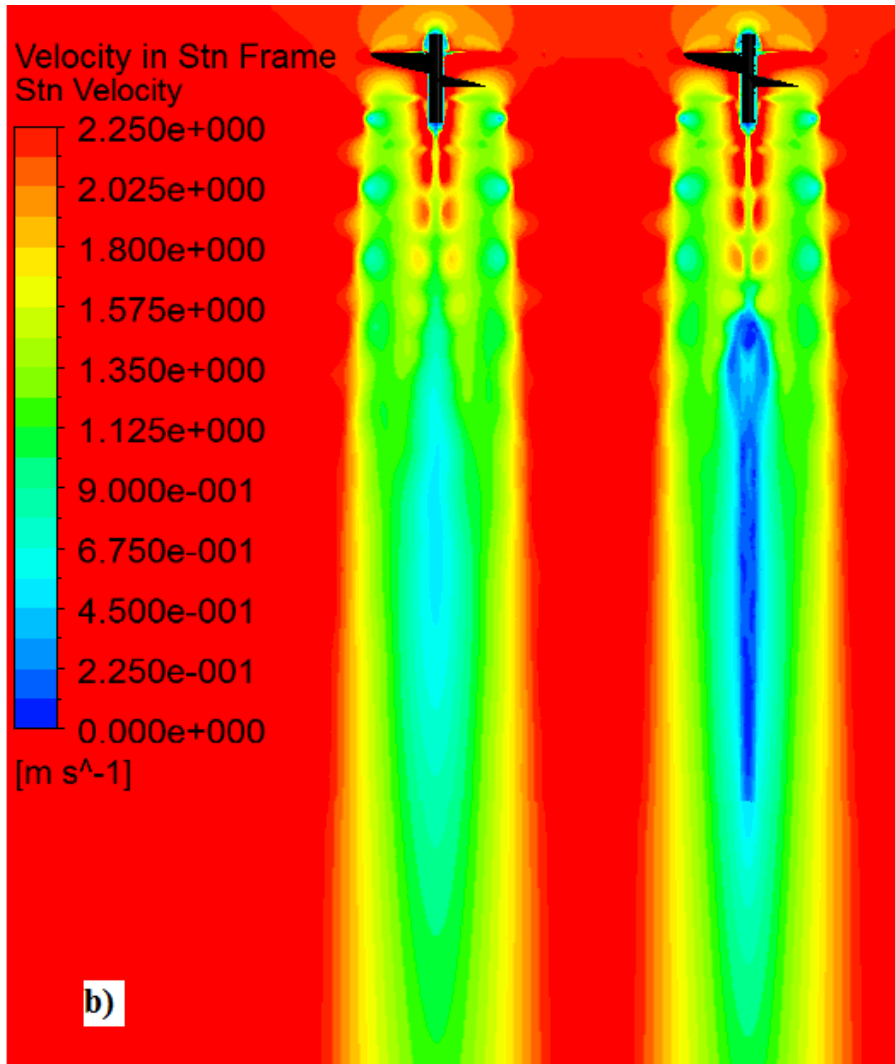
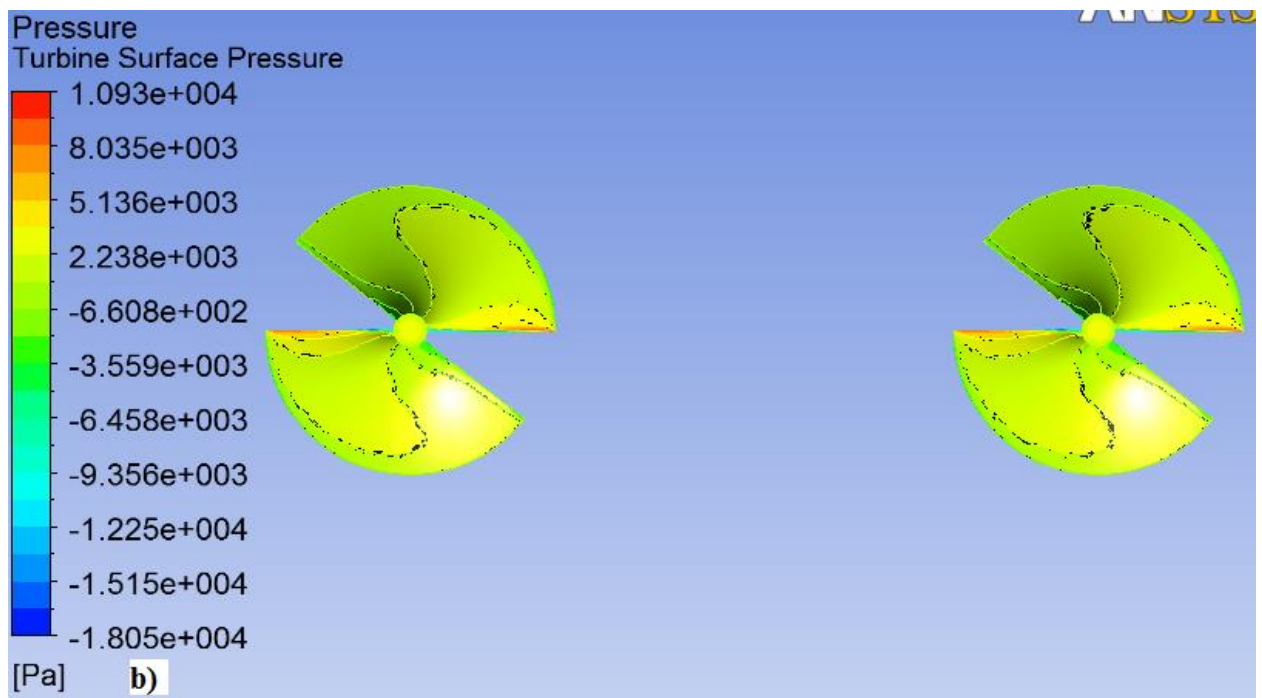**Figure 16: Velocity Downstream of Turbines for a) Fine Mesh and b) Coarse Mesh at d = 5R**
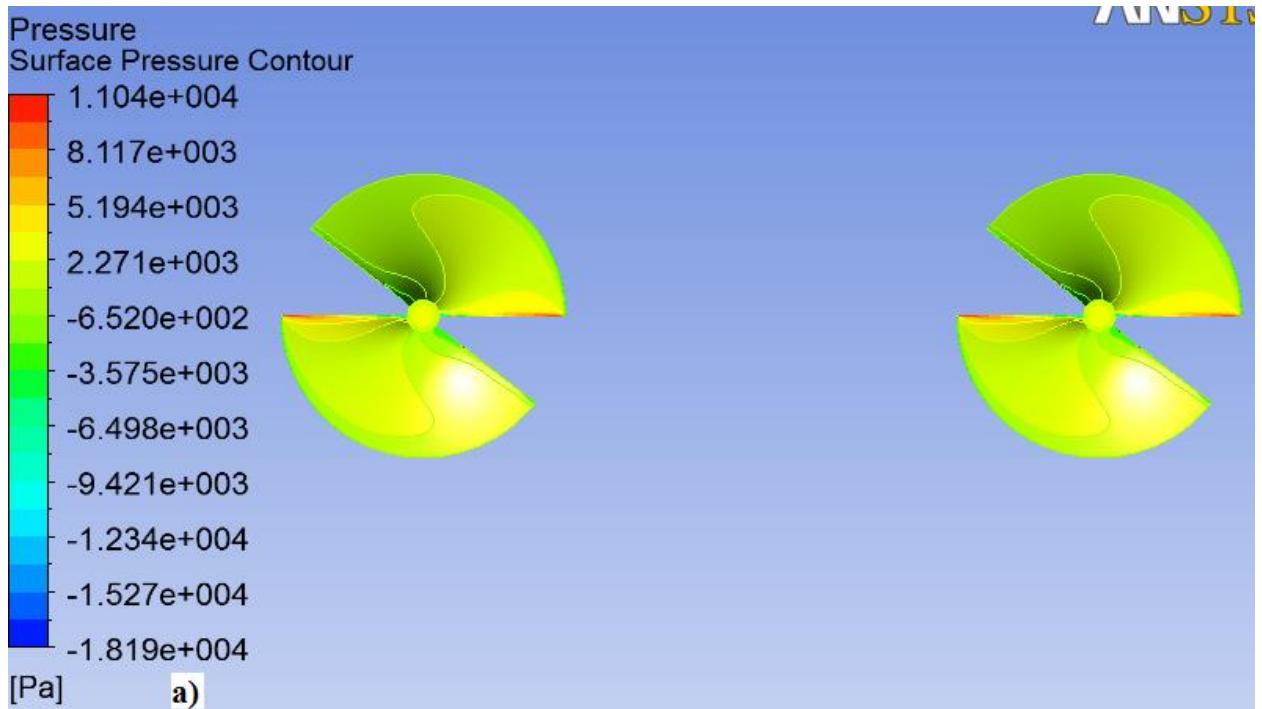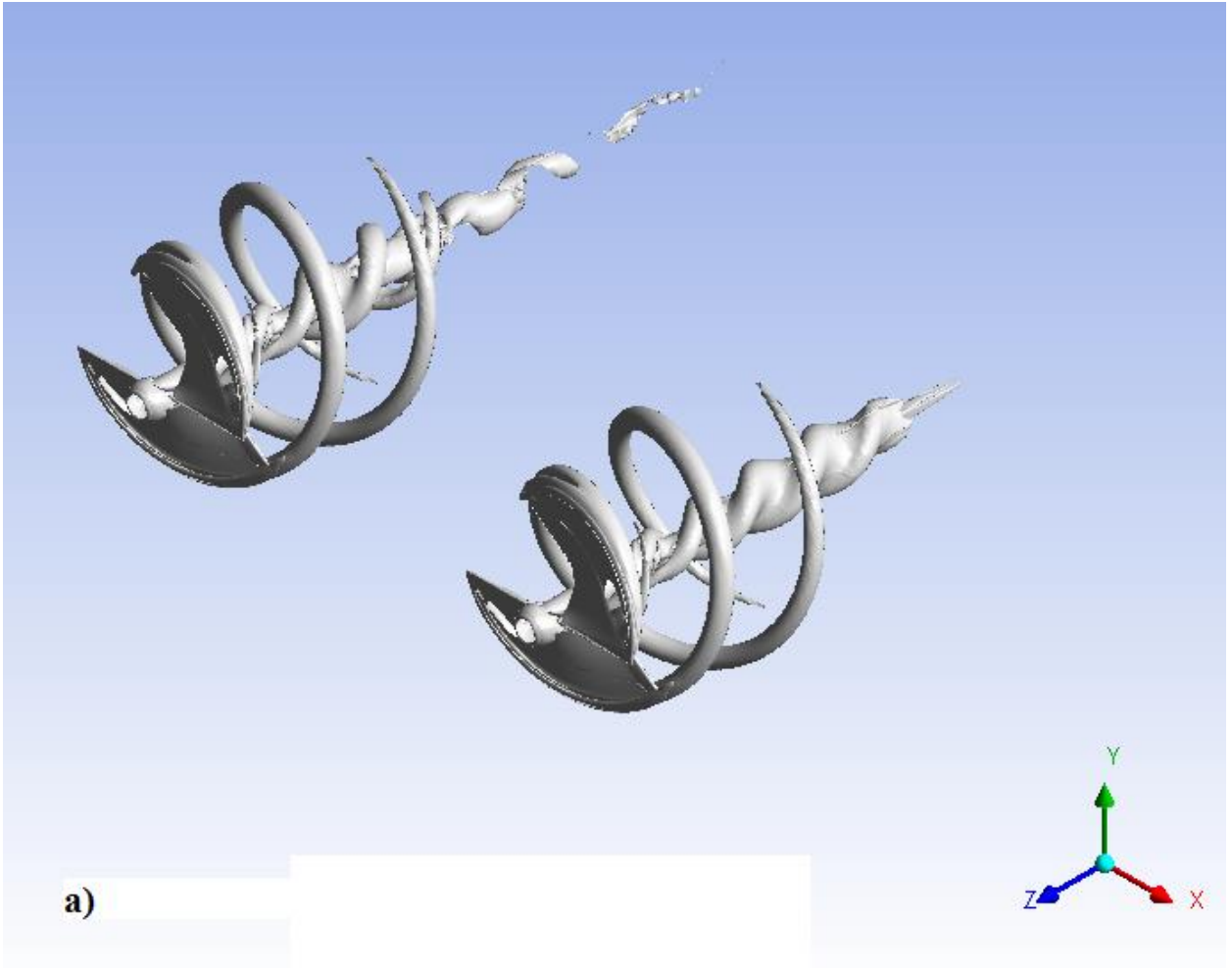
Figure 17: Surface Pressure Contours for d = 5R separation distance on a) Fine Mesh and b) Coarse Mesh
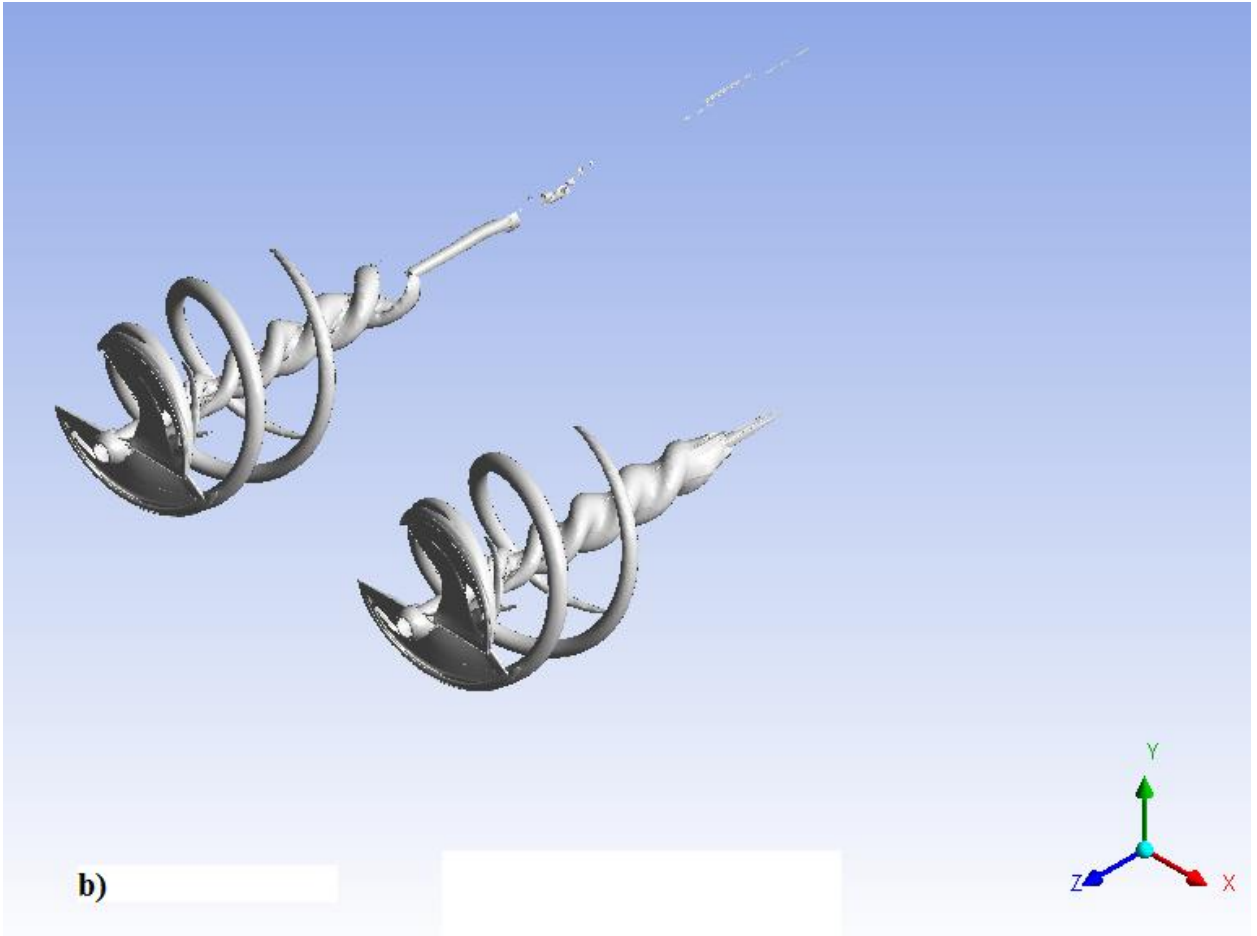
a)

Figure 18: Surface of Constant Vorticity (25.25 s^-1) for d=5R on the a) Fine Mesh and b) Coarse Mesh

Notice in these plots several features of the flow that should be expected. In figures 16 and 18, the vortex shedding effects at the blade tips and blade hub are well defined for both mesh sizes. Likewise in Figure 17 the upstream side of the blade leading edge is seen to have the highest pressure, and (although not shown in these plots) the downstream side of the blade leading edge has the lowest pressure. All of these flow characteristics are clearly defined in both the coarse mesh and fine mesh simulations, which provides evidence that any relationship between the power/drag and the separation

47

distance is not due to a meshing anomaly. This can help to provide confidence that the trends found in this study between the relevant parameters are accurate.
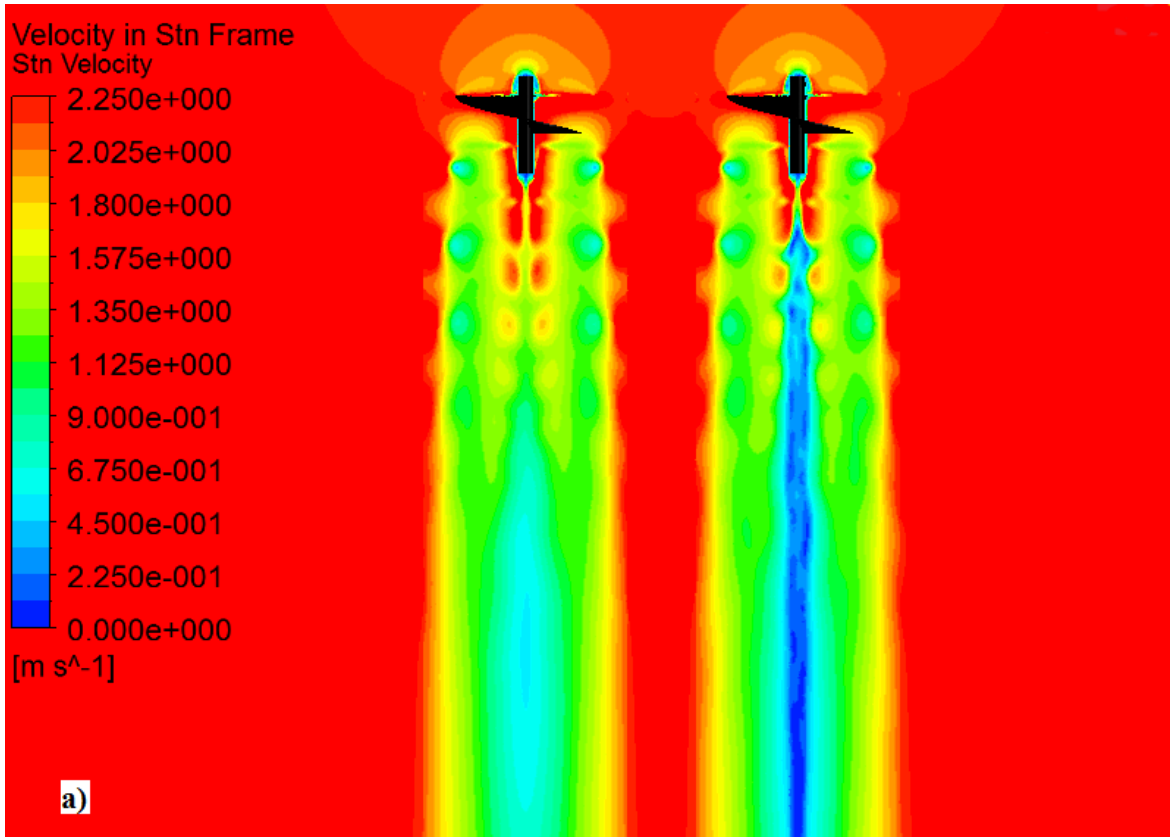
The residuals for each simulation are shown below in figure 19; these numbers represent the highest converged residual around which the discretized mesh and specified solver converged to and fluctuated around.
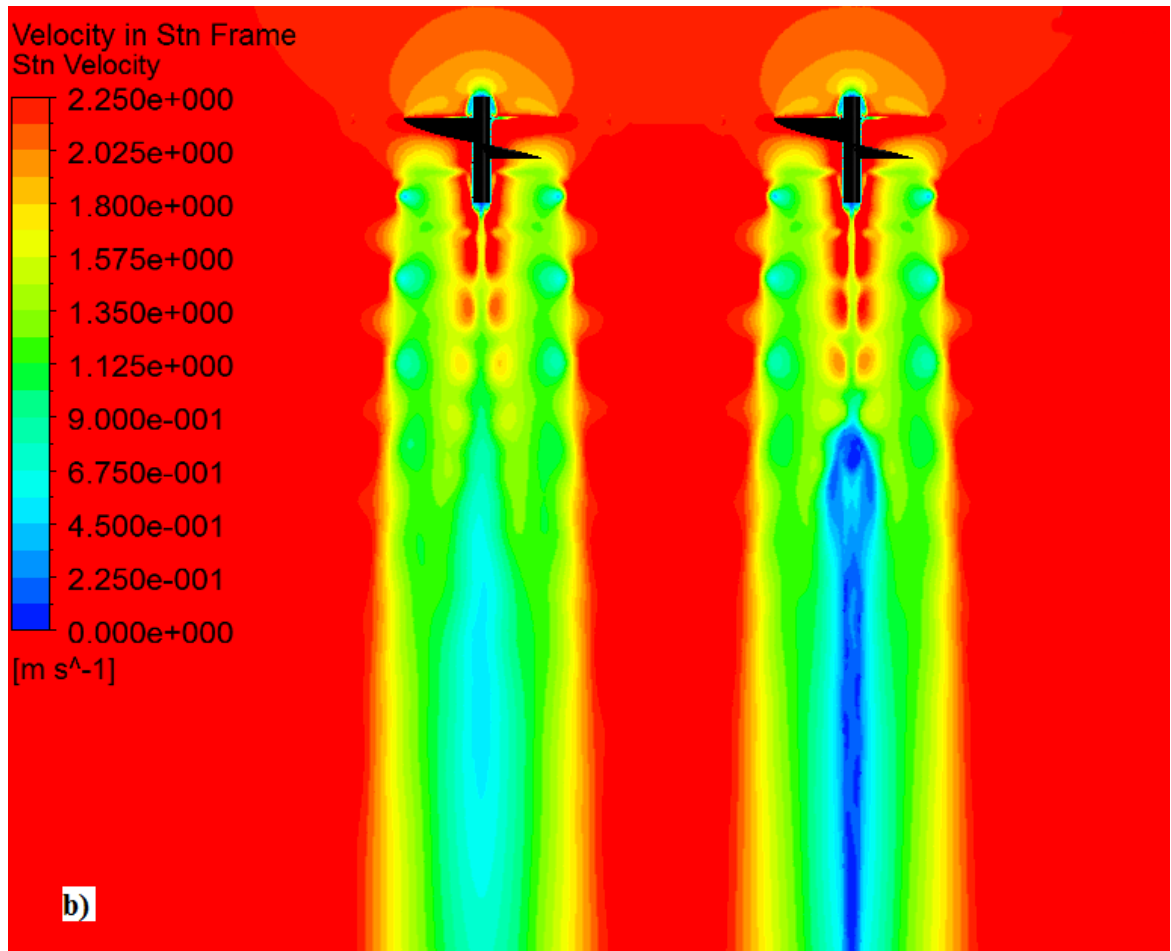
		3R	4R	5R	6R	7R
Highest Residual	Fine Mesh	7.53E-05	2.95E-04	4.62E-05	-	-
	Coarse Mesh	1.72E-04	2.29E-04	7.94E-05	6.04E-05	1.81E-05

Figure 19: Highest Residual for each Simulation

For HAHKT's, a convergence criterion for the residuals of less than 10^{-4} can be used [12]. Unfortunately, not all simulations in the present study were able to meet this goal due a combination of mesh size/aspect ratio limitations. However, even though some simulations were unable to meet this maximum allowable residual criterion, the power and drag coefficients can be shown to converge for a given mesh well before any residual criterion is met. This confirms that even though the residuals might not be where they ideally should be, the drag and moment coefficients that are found are not changing with any noticeable precision after a certain point in the residual convergence. Therefore, the solutions found can be expected to accurately represent expected turbine performance at that separation distance even without satisfying these residual criteria.

As discussed in the previous section, it is also valuable to investigate the velocity and pressure contours of the results that are generated. There were a total of eight different simulations run in this study, so it would be impractical to list all of those contours for every simulation. Shown in figures 20 and 21 are the velocity contours and a surface of constant vorticity for the coarse d = 3R, d = 5R, and d=7R simulations.

48

Velocity in Stn Frame
Stn Velocity

2.250e+000
2.025e+000
1.800e+000
1.575e+000
1.350e+000
1.125e+000
9.000e-001
6.750e-001
4.500e-001
2.250e-001
0.000e+000
[m s^-1]

a)

Velocity in Stn Frame
Stn Velocity
2.250e+000
2.025e+000
1.800e+000
1.575e+000
1.350e+000
1.125e+000
9.000e-001
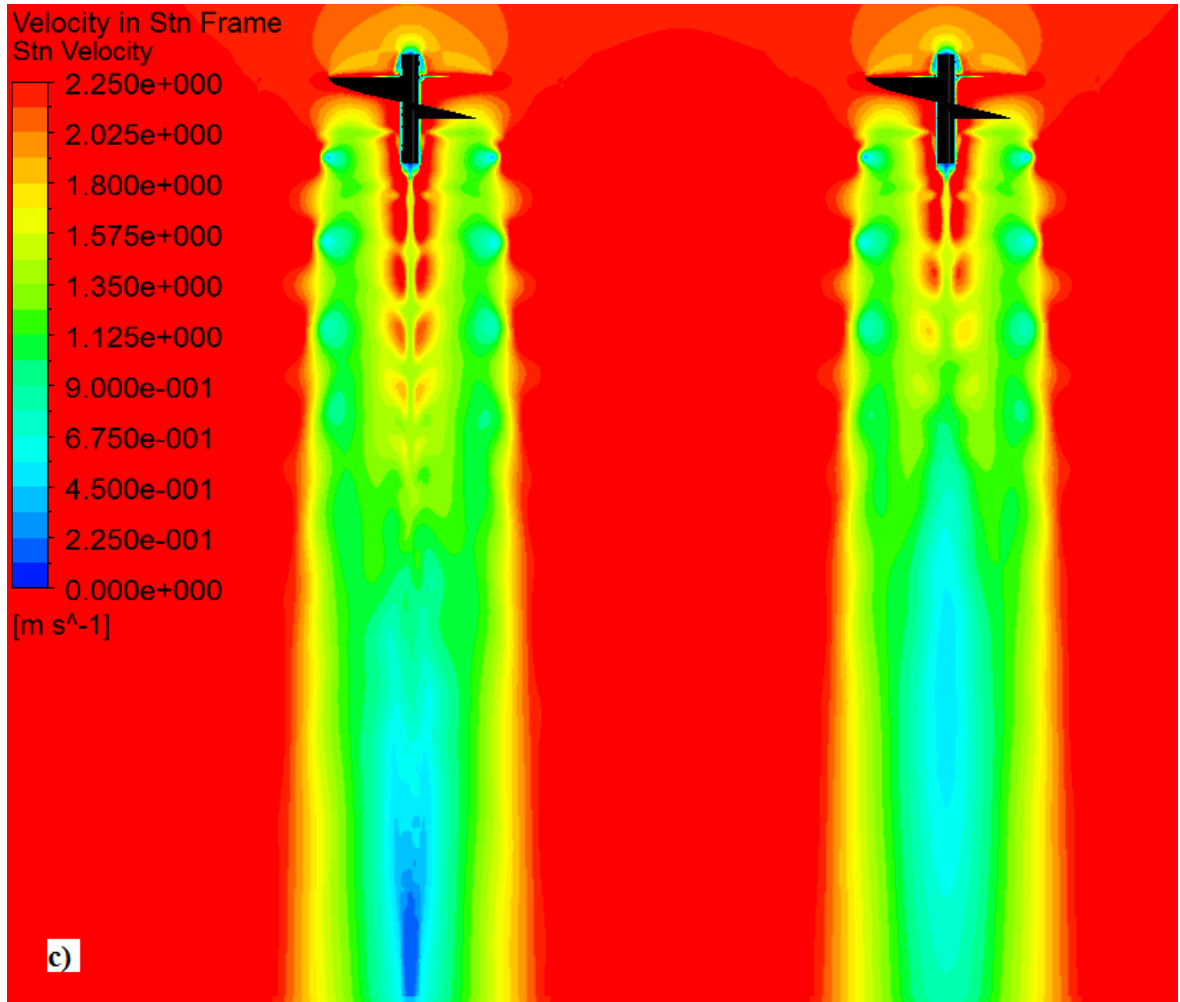6.750e-001
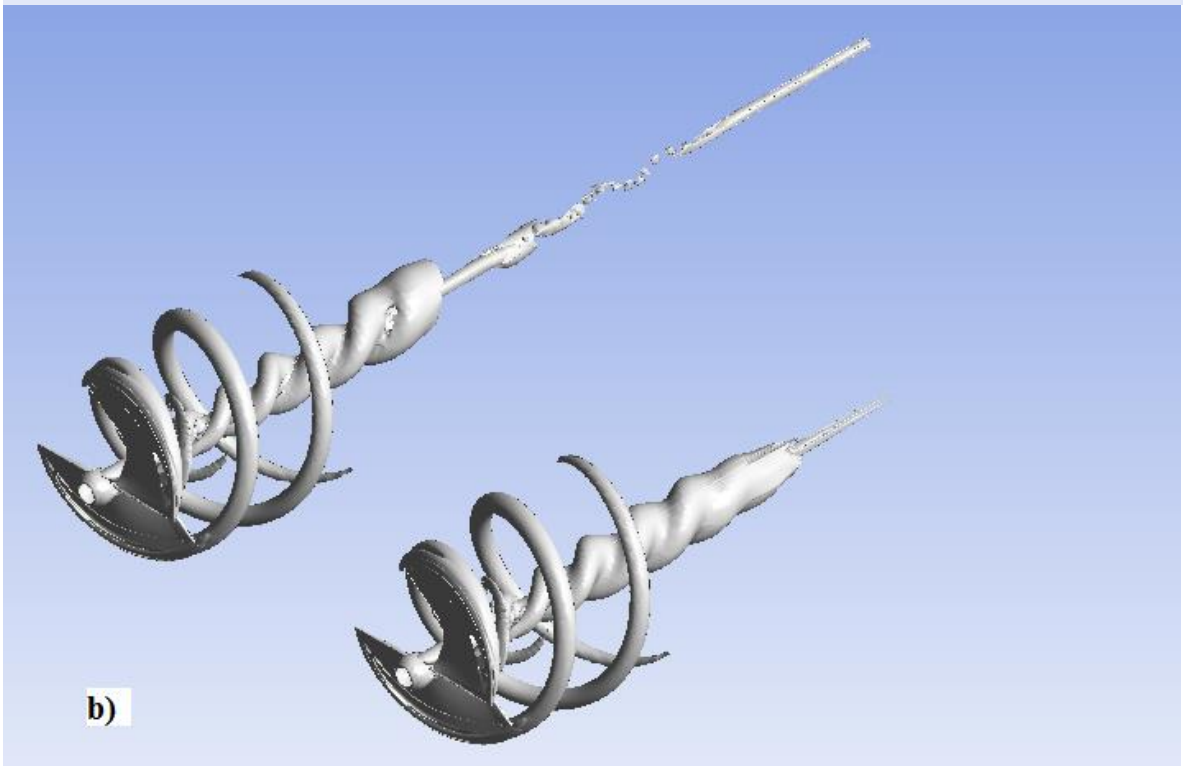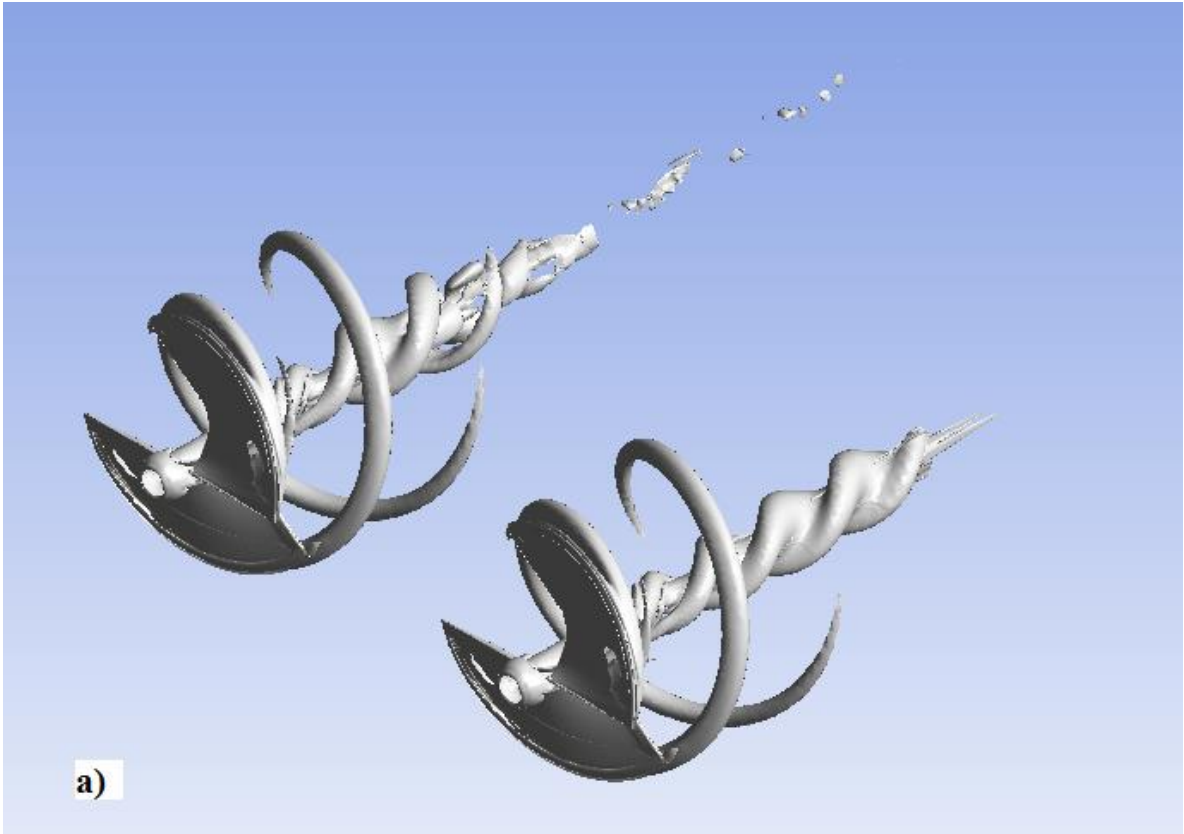4.500e-001
2.250e-001
0.000e+000
[m s^-1]

b)

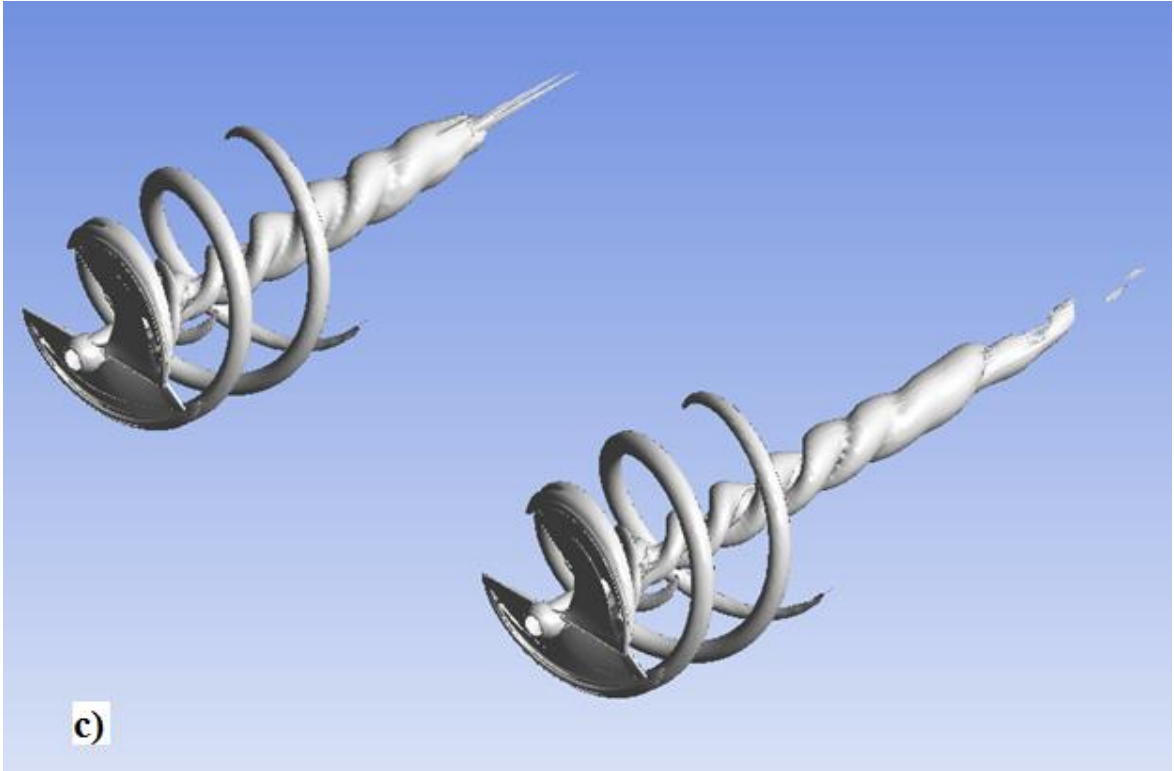**Figure 20: Velocity Contours on Coarse mesh for the a) d = 3R b) d = 5R and c) d = 7R simulations**

a)

b)

Figure 21: Surfaces of Constant Vorticity on the coarse mesh for a) d = 3R b) d = 5R and c) d = 7R simulations

From these plots, it can be seen that the wakes behind the turbines in each simulation look very similar at each separation distance. This is to be expected, as the turbines used in all simulations and the free stream velocity/boundary conditions are the same. Because of this similarity, these plots only serve to provide more confidence in this computational study's results.

The final method of verifying solution accuracy is to make sure that the blades of the turbines are undergoing flow conditions that the turbulence model that was selected is suitable for. As discussed in the previous section, this is done by investigating the y^+ values on the blade surface. Plotting that value over the 30 to 300 range on the turbines, as shown in figure 22 for the d=5R separation distance, shows smooth y^+ value contours.
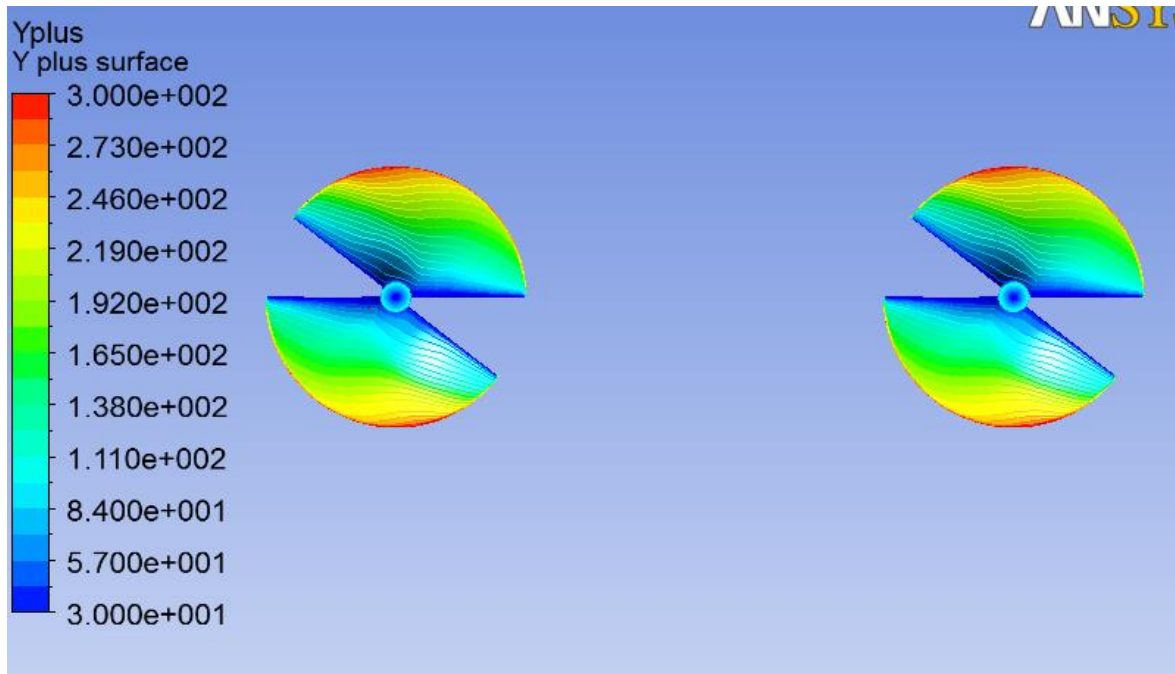
Figure 22: y^+ values for the coarse mesh d = 5R simulation

The y^+ contours on the turbine surface shown in Figure 22 show that the flow conditions around each turbine are captured very well by the k-ω SST turbulence model and by the mesh that was used at each surface. This means that this turbulence model has been experimentally verified for flow conditions similar to those in the present study, providing even more confidence in the accuracy of the predicted results.

The y^+ contours for the other mesh sizes and other separation distances look essentially identical to the ones shown in figure 22, and are not attached in this paper to avoid pictorial redundancy.

4.   Conclusion

4.1 Results Summary and Turbine Placement Recommendations

The effects of separation distance between two turbines on each turbine's drag coefficients, performance coefficients, and on the resulting flow characteristics were studied. In order to maximize both combined turbine power output and resultant drag for both turbines, the simulation results suggest that, in a uniform flow field, the turbines should be placed as far apart as is feasible. At every separation distance, the drag and performance coefficients of the left and the right turbines are shown to be very similar.

In reality a river will not have a uniform flow distribution; in fact, the flow of many rivers has been measured by geologists and they tend
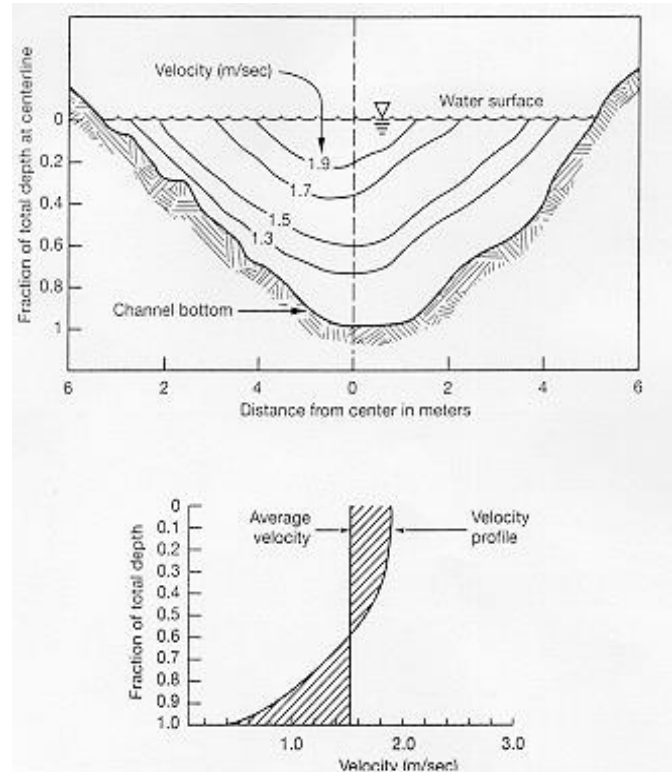
Figure 23: Typical river flow cross-section [23]

to have a velocity distribution similar to what is shown in Figure 23. For those in the field who wish to maximize turbine power output, the turbines should be placed in the river cross section in a manner that maximizes the kinetic energy of the water that enters those turbines. As seen in Figure 23, the maximum kinetic energy of the river will be found in a region close to the river's surface, so it makes sense to place the turbines in that region.

55

However it is also important to realize that, inside of this high-velocity region, the gradient of the velocity vector will be near zero and the flow can therefore be considered approximately uniform. If this is the case, then the results of this study would still hold as long as the turbines are placed within that high fluid velocity and near-zero gradient region.

Additional restrictions on turbine placement become apparent due to the realization that, if the turbines are placed too close to the surface, there will be two-phase air and water interaction. The single-phase simulations done in this study are unable to take into account the mixing of air and water that occurs in the form of periodic surface waves, generated air bubbles in the fluid, and water droplets which can be expelled momentarily from the river's surface. In addition to being much more difficult to model, the air-water interaction is also not something that the eventual customers of these turbines will want, as it will almost assuredly increase turbine wear and decrease turbine performance. Therefore, the turbines should be placed sufficiently beneath the river's surface so that this detrimental air-water interaction never manifests itself.

The results of this study therefore suggest that the turbines should be placed far apart from each other within the high-velocity region near the top-center of the river's cross section. But, because of air-water interactions, the author recommends that the turbines also be placed sufficiently far below the free surface of the river in order to maximize the system's power output.

4.2 Physical Explanation of Simulation Results

From a purely fluid mechanics intuition standpoint, if two turbines are put very close together, it can be expected that their flows would interact downstream. This interaction is a result of the turbines interfering with the development of each other's wake, and would make the turbine's flow develop less "easily" in comparison to how they would behave in the free stream. Therefore, it makes sense that the presence of two turbines adjacent to one-another in a stream would negatively impact the drag and performance coefficients of each other. Looking back at figures 13 and 14, it can be shown that the power and drag coefficients done in this study at the smaller separation distances match up nicely with this intuition.

Using this as a starting point, then it can be deduced that, as the turbines are separated further and further, the degree of interaction between the two turbines wakes would be reduced. This suggests that the power and drag of each turbine should asymptotically approach some maximum value as this separation distance in increased. The results from this study do show the power and drag coefficients beginning to level off at a larger separation distance, which confirms this intuition.

It can then be concluded that many of the trends discovered through this study do match up neatly with what those with a strong fluid mechanics background should expect them to be. This provides further evidence that, although certainly not without its imperfections, the results presented in this study can be assumed to be of reasonable accuracy.

4.3 Methods of Simulation Validation

The limited computational and temporal resources at the author's disposal leave plenty of opportunity for further study on this problem. In order to validate the results presented in this thesis, the author recommends the use of fully transient simulations to verify that the steady-state assumptions used in the present study are succeeding in capturing all important flow characteristics. The inherently unsteady nature of the flow as well as the extent of turbulent interaction between each turbine means that this problem should benefit greatly from the improved accuracy associated with a transient simulation.

However, even the use of a transient simulation cannot correct for the limitations that this particular experiment places on the size of the rotating domains around each turbine. As of the conclusion of this study, the affect that the changing size of the rotating domain has on the results of the present simulations is unknown. This can be rectified by performing a study on the effect of the rotating domain size on the predicted turbine performance, and then by comparing those results to the ones in this study.

A way to circumvent dealing with the unknown effect of the rotating domain is to get rid of the cylindrical rotating domains entirely and instead model the rotation of each turbine via an adaptive meshing scheme. Instead of rotating the cylindrical mesh a small amount with each time step, the turbine geometry itself is rotated within a larger body during each time step, and the domain around both turbines would need to be meshed again at every time step. This is only possible through the creation of an unstructured adaptive meshes near the turbine blades, which creates several computational hurtles that the present study was able to go around addressing. Naturally, the researcher would need

to have extensive computational resources at their disposal in order to make such a study feasible.

Alternatively, experimental studies should be done in water tunnels to provide further validation for the results presented in this study. Nonetheless, this study should prove to be a worthwhile foundation for further research in this area, as well as provide a guide to those who seek to maximize turbine performance in a real river.

4.4 Areas of Further Research

As stated in earlier sections, the present study only modeled a single fluid, the water, in order to determine turbine performance. This is a valid assumption as long as the turbines are placed well beneath the river surface, but when the turbine is rotating near the river's surface this may not be the case due to air and water mixing. This is a phenomenon that the present simulations have not even attempted to model, but the presence of air hitting the turbine blades instead of water would almost assuredly negatively affect turbine performance and increase turbine wear. In a more academic sense, the scale of how large this decrease in performance will be as a function of the turbine's distance beneath the river's surface is still unstudied. Therefore, further research on this subject could include modeling both the air and the water in order to discover this relationship as well as shed light on just how far beneath the surface the turbines should be placed.

More research could also be done to further optimize turbine performance over a wider range of tip speed ratios. Such research may include changing the blade pitch and/or blade rotation rate, increasing the number of blades, varying the thickness of the

blades to a more streamlined cross-section, or even creating adjustable-pitch turbine blades (similar in concept to Kaplan turbines used in many modern hydroelectric dams).

Alternative areas of research could involve including more of the turbine system into the CFD simulations. The present study used only the turbine blades and turbine hub geometry to derive system performance, but did not attempt to model the nacelle that will be attached to the turbine (in order to house the gear box and generator) or model the mooring of the turbine system (to hold the system in place in the river). Naturally, taking these factors into account would simultaneously increase the complexity of the simulations, but could also better represent the conditions in which the turbines will be deployed.

Bibliography

[1]   *Hydroelectric Power*. Tennessee Valley Authority. [Online]
http://www.tva.gov/power/hydroart.htm (Accessed Mar 14, 2014).

[2]   Hayley Moller, *Data Highlights*. Earth Policy Institute. Published: Jun 14, 2012.
[Online] http://www.earth-policy.org/data_highlights/2012/highlights29 (Accessed
March 18, 2014)

[3]   *Environmental Costs of Electricity*, Pace University Center for Environmental and
Legal Studies (Oceana Publications, 1990) [Online]
http://www.stewartmarion.com/carbon-footprint/html/carbon-footprint-kilowatt-
hour.html#carbon-dioxide-from-one-kilowatt-hour (Accessed April 2, 2014).

[4]   *Use and Capacity of Global Hydropower Increases.* Worldwatch Institute.
[Online] http://www.worldwatch.org/node/9527 (Accessed April 2, 2014).

[5]   *About Wind Energy*. Continental Wind Power. [Online]
http://mstudioblackboard.tudelft.nl/duwind/Wind%20energy%20online%20reader
/figures/horizontal_vertical.gif (Accessed April 9, 2014).

[6]   V.B. Miller, L.A. Schaefer. *Computational Fluid Dynamics for Hydrokinetic
Turbines.* Proceedings of the ASME 2009 International Mechanical Engineering
Congress and Exposition. IMECE2009-11115. November 13-19, Lake Buena Vista,
Florida, USA.

[7]   N. Kolekar, Z. Hu, A. Banerjee, X. Du. *Hydrodynamic Design and Optimization
of Hydro-kinetic Turbines using a Robust Design Method*. Proceedings of the 1st Marine
Energy Technology Symposium. April 10-11, 2013, Washington, D.C. pp 8

[8]   *Millennium Problems*. Clay Mathematics Institute. [Online]
http://www.claymath.org/millennium-problems (Accessed April 15, 2014).

[9]   *Direct Numerical Simulation*. CFD Online. [Online] http://www.cfd-
online.com/Wiki/Direct_numerical_simulation_%28DNS%29 (Accessed April 15, 2014)

[10]   D.C. Wilcox. *Turbulence Modeling for CFD*. Third Edition (DCW Industries,
Inc., La Canada, CA 2010) pp. 4, 108-109, 16.

[11]   *Statement on the Control of Numerical Accuracy*. ASME Journal of Fluids
Engineering. http://journaltool.asme.org/templates/JFENumAccuracy.pdf

[12]   S.S. Mukherji, N. Kolekar, A. Banerjee, and R. Mishra. *Numerical Investigation
and evaluation of optimum hydrodynamic performance of a horizontal axis hydrokinetic
turbine*. Journal of Renewable and Sustainable energy **3**, 06315 (2011); doi:
10.1063/1.3662100

[13]   B. Gunawan, V.S. Neary, C. Hill, and L.P. Chamorro. "Measurement of velocity
deficit at the downstream of a 1:10 axial hydrokinetic turbine model." Energy-Water-
Ecosystems Engineering, Wind and Power Technologies, Environmental Sciences
Division, Oak Ridge National Laboratory. http://energy.sandia.gov/wp/wp-
content/gallery/uploads/velocitydeficit_neary.pdf

[14]   W. C. Schleicher, J. D. Riglin, Z. A. Kraybill, A. Oztekin and R. C. Klein, Jr.,
"Design and Simulation of a Micro Hydrokinetic Turbine," in *Proceedings of the 1st
Marine Energy Technology Symposium*, Washington, D.C., 2013.

[15]   M. Zadravec, S. Basic, M. Hribersek. "The Influence of Rotating Domain Size in
a Rotating Frame of Reference Approach for Simulation of rotating Impeller in a Mixing

Vessel" in *Journal of Engineering Science and Technology*. Vol. 2, No. 2 (2007) 126 – 138 © School of Engineering, Taylor's University College

[16]   *Navier-Stokes Equations – Rotational*. Wolfram Research. [Online] http://scienceworld.wolfram.com/physics/Navier-StokesEquationsRotational.html (Accessed May 1, 2014)

[17]   F.R. Menter, "Two-equation Eddy-Viscosity Turbulence Models for Engineering Applications," *AIAA Journal*, Vol. 32, no. 8, pp. 1598-1605, August 1994.

[18]   *Turbulence Free-stream Boundary Conditions*. CFD Online. [Online]. http://www.cfd-online.com/Wiki/Turbulence_free-stream_boundary_conditions (Accessed May 3, 2014)

[19]   *Turbulence Intensity*. CFD Online. [Online]. http://www.cfd-online.com/Wiki/Turbulence_intensity (Accessed May 3, 2014)

[20]   *Turbulent Length Scale*. CFD Online. [Online] http://www.cfd-online.com/Wiki/Turbulent_length_scale (Accessed May 3, 2014)

[21]   *Dimensionless Wall Distance*. CFD Online. [Online] http://www.cfd-online.com/Wiki/Dimensionless_wall_distance_%28y_plus%29 (Accessed May 3, 2014)

[22]   *FLUENT 14.0 User's Guide*. ANSYS http://cdlab2.fluid.tuwien.ac.at/LEHRE/TURB/Fluent.Inc/v140/flu_ug.pdf

[23]   *Environmental Techniques – Stream Discharge Measurement*. University of Colorado, Department of Geography. [Online]. http://www.colorado.edu/geography/courses/geog_2043_f01/lab01_2.html (Accessed Jun 6, 2014)

Vita

Joseph David Jonas was born on February 23, 1991 to Gordon M and Cynthia J Jonas in Fairfield, Connecticut. Since then he has had the fortune of living in many different places early in his life, which in addition to his place of birth include the outskirts of Knoxville, Tennessee; Charlotte, North Carolina; Corning, New York; and Allentown, New Jersey, where he graduated from Allentown High School class of 2009. Since then, he attended Lehigh University for his Bachelor of Science degree in Mechanical Engineering, a degree which he received with high honors in January of 2013. Upon the completion of his B.S. and with the aid of Lehigh's Presidential Scholar program, Joseph started pursuing his Masters of Science degree in Mechanical Engineering, of which this Thesis is the final requirement.